Momentum-transfer-squared distributions are shown for three particle combinations in Fig. 22. The t_{KK^*} distribution is well described by the model. The agreement with the $t_{K^-\pi^-}$ distribution is reasonable at large t but there is an apparent disagreement for low values of $t_{K^-\pi^-}$, where the model predicts a larger number of events than actually occur. The distribution of the quantity $t_{dd}-t_{\min}$ again shows reasonable agreement with the model.

The polar and azimuthal distributions of the normal to the decay plane of the $K\pi\pi$ system are seen in Fig. 23, with good agreement between the data and the model. This is a result of the assumption of a dominant $\cos^2\theta$ dependence for the decay angular distribution of the $K^-\pi^+$ system as well as the s-wave $\bar{K}^*\pi$.

The $\pi^+\pi^-$ mass distribution and the decay angular distribution of the $\bar{K}^*$ helicity angle θ_H are shown in Fig. 24. The $\pi^+\pi^-$ mass spectrum shows an excess of events in the ρ region above the prediction of the model. An excess of similar magnitude above the isotropic distribution predicted by the model for the helicity angle is seen for $\cos\theta_H$ near 1.0. Ignoring complications due to crossing $\bar{K}^*$ and ρ bands, we estimate the amount of ρ present to be about 10% of the sample.

The $(d\pi^+)$ mass distribution predicted by the model is shown by the solid curve in Fig. 25. The shape of this distribution is seen to be strongly influenced by the reflection of the $\bar{K}^{*0}$ decay, which produces broad enhancements at both low and high masses, particularly the former.

The double-Regge-pole model gives a good fit to the gross characteristics of our data. This in no way excludes the possibility that one or more resonances may occur in the low-mass $\bar{K}^*\pi$ enhancement. According to the duality hypothesis, the t-channel process calculated above could described the average behavior of perhaps several closely spaced resonances.

V. CONCLUSIONS

We have studied the production and decay characteristics of the Q enhancement produced in the reaction $K^-d\to K^-\pi^-\pi^+d$. We find no evidence for mass structure within this enhancement. The spin-parity assignment is found to be mainly $J^P=1^+$. In agreement with previous experiments which observe K^{*0} production, our data indicate the polar-angle decay distribution with respect to the beam direction to have a marked asymmetry. We further observe the mass dependence of the spherical harmonic moments of the $K^-\pi^+$ decay distribution to be in striking agreement with that observed in the reaction $K^+\pi\to K^+\pi^-\Delta^{++}$. An explanation of this asymmetry requires the presence of a $J^P=0^-$ $K\pi\pi$ system throughout the Q region. The Reggeized Deck model is found to provide an acceptable description of most features of our data.

ACKNOWLEDGMENTS

We thank the operating crews of the ZGS and of the 30-in. bubble chamber for their cooperation, and also our scanning and measuring staff for their careful work.

PHYSICAL REVIEW VOLUME 188, NUMBER 5 25 DECEMBER 1969

Experimental Study of the Decay $K_L\to\pi^0\pi^0$ and Other Rare Decay Modes*†

M. BANNER,‡ J. W. CRONIN, J. K. LIU,§ AND J. E. PILCHER‖
Palmer Physical Laboratory, Princeton University, Princeton, New Jersey 08540
(Received 8 August 1969)

We have measured the branching ratio $\Gamma(K_L\to 2\pi^0)/\Gamma(K_L\to 3\pi^0)$ to be $(4.6\pm1.1)\times10^{-3}$. This leads to $\Gamma(K_L\to 2\pi^0)/\Gamma(K_L\to\text{all})=(0.97\pm0.23)\times10^{-3}$ and a CP-violation parameter $|\eta_{00}|=(2.2\pm0.3)\times10^{-3}$. We also report $\Gamma(K_L\to\gamma\gamma)/\Gamma(K_L\to\text{all})=(4.7\pm0.6)\times10^{-4}$, $\Gamma(K_S\to\gamma\gamma)/\Gamma(K_S\to\text{all})<0.02$ with 90% confidence and $\Gamma(K_L\to\pi^0\gamma\gamma)/\Gamma(K_L\to\text{all})<2.3\times10^{-4}$ with 90% confidence.

I. INTRODUCTION

THE discovery of the decay mode $K_L\to\pi^+\pi^-$ [1] has led to extensive experimental study of the neutral-K-meson system.[2] At present, the experiments strongly indicate a violation of CP symmetry.[3] Extensive efforts to find CP nonconservation and T violation in systems other than the neutral K system

* Work supported by the U. S. Office of Naval Research, under Contract No. N0014-67-A-0151-0001, and by the U. S. Atomic Energy Commission, under Contract No. AT(30-1)-2137. This work also made use of computer facilities supported in part by National Science Foundation Grant Nos. NSF-GJ-34 and NSF-GU-3157.

† Further details on this work appear in the doctoral theses of two of the authors (J. K. L. and J. E. P.), Technical Reports 48 and 49, Elementary Particles Laboratory, Princeton University (unpublished).

‡ On leave from Département de Physique des Particules Elementaires, Centre d'Etudes Nucléaires, Saclay, France.

§ Present address: Stanford Linear Accelerator Center, Stanford, California 94305.

‖ Present address: CERN, 1211 Geneva 23, Switzerland.

[1] J. H. Christenson, J. W. Cronin, V. L. Fitch, and R. Turlay, Phys. Rev. Letters **13**, 138 (1964).

[2] There have been many excellent reviews of the experimental situation for K decay. See, e.g., L. B. Okun and C. Rubbia, in *Proceedings of the International Conference on Elementary Particles, Heidelberg, 1967*, edited by H. Filthuth (North-Holland Publishing Co., Amsterdam, 1968), p. 301.

[3] P. K. Kabir, Phys. Rev. Letters **22**, 1018 (1969); P. Darriulat, J. P. Deutsch, K. Kleinknecht, C. Rubbia, and K. Tittel, Phys. Letters **29B**, 132 (1969).

have so far failed to uncover any such violations.[4] Thus, a detailed study of the neutral-K-meson system seems to be the most fruitful approach towards understanding CP violation.

We describe in this paper a measurement of the CP-violating decay rate $K_L \to 2\pi^0$. We also present rates or upper limits on the following decay modes: $K_L \to \gamma\gamma$, $K_S \to \gamma\gamma$, and $K_L \to \pi^0\gamma\gamma$. The results for the rates $K_L \to 2\pi^0$ and $K_L \to \gamma\gamma$ have already been published in abbreviated form.[5]

The phenomenology of the neutral-K system has been extensively discussed in the literature.[6] We outline below the main results of the analysis which assumes CPT invariance. The degeneracy of the states K^0 and $\bar{K}^0$ under the strong and electromagnetic interactions is lifted by weaker interactions, so that the neutral K

$$|K_S\rangle = \frac{p|K^0\rangle + q|\bar{K}^0\rangle}{(|p|^2+|q|^2)^{1/2}}$$

and

$$|K_L\rangle = \frac{p|K^0\rangle - q|\bar{K}^0\rangle}{(|p|^2+|q|^2)^{1/2}}. \quad (1)$$

The complex parameters p and q are determined by a conventional perturbation treatment. The important observable amplitude ratios which indicate the strength of the CP violation in this system are

$$\eta_{+-} = \frac{\langle\pi^+\pi^-|H|K_L\rangle}{\langle\pi^+\pi^-|H|K_S\rangle} \quad \text{and} \quad \eta_{00} = \frac{\langle\pi^0\pi^0|H|K_L\rangle}{\langle\pi^0\pi^0|H|K_S\rangle}, \quad (2)$$

where H is the interaction Hamiltonian. They satisfy the relations

$$\eta_{+-} = \epsilon + \epsilon', \quad \eta_{00} = \epsilon - 2\epsilon', \quad (3a)$$

where

$$\epsilon = (p-q)/(p+q),$$

$$\epsilon' = \frac{i}{\sqrt{2}} \frac{\mathrm{Im}(A_2)}{A_0} e^{i(\delta_2-\delta_0)}, \quad (3b)$$

and $A_I e^{i\delta_I}$ is the K^0 transition amplitude to an outgoing $\pi\pi$ state of isospin I. The parameter ϵ denotes the contribution to the CP violation from the composition of the decaying states, while ϵ' gives the contribution from a T violation in the $K \to \pi\pi$ amplitudes.

The principal goal of this experiment was to determine $|\eta_{00}|$. We have measured the branching ratio $\Gamma(K_L \to \pi^0\pi^0)/\Gamma(K_L \to 3\pi^0)$ which yields $|\eta_{00}|$ when combined with well-established experimental data on the decay rates $\Gamma(K_L \to 3\pi^0)$ and $\Gamma(K_S \to \pi^0\pi^0)$. The central problem of the measurement was to separate the decay $K_L \to \pi^0\pi^0$ from $K_L \to \pi^0\pi^0\pi^0$ which is some 200 times more probable. The poor signal-to-noise ratio was largely overcome by using the fact that the γ-ray energy spectra in the K_L center-of-mass system ($E_{\text{c.m.}}$spectra) are distinctly different for the two decays (Fig. 1). Specifically, the γ-ray energy spectrum from $3\pi^0$ decay has an upper limit at 165 MeV, while that for $2\pi^0$ decays extends to 229 MeV. An apparatus was constructed which was most sensitive in the energy region accessable only to γ rays from the $2\pi^0$ decay ($E_{\text{c.m.}} = 165$–229 MeV), and relatively insensitive in the 3π region, $E_{\text{c.m.}} < 165$ MeV. This apparatus also allowed a search for other rare neutral-K decay modes which have a γ-ray $E_{\text{c.m.}}$ spectrum extending beyond 165 MeV.

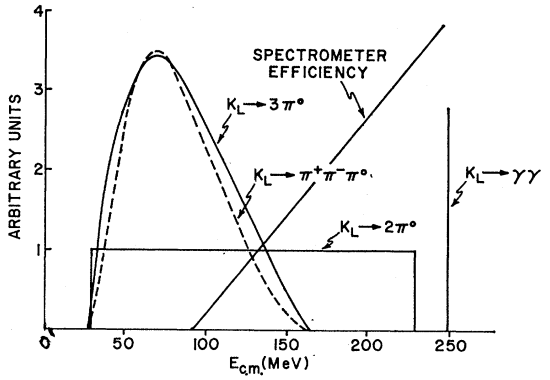

FIG. 1. Energy spectra for γ rays from the $K_L \to 3\pi^0$, $\pi^+\pi^-\pi^0$, $2\pi^0$, and $\gamma\gamma$ decay modes in the K_L c.m. system. The relative detection efficiency of the spectrometer for a single γ ray is also shown.

II. EXPERIMENTAL APPARATUS AND DATA COLLECTION

The experiment was performed at the Princeton-Pennsylvania Accelerator. The 3-BeV protons struck an internal platinum target for 8 msec, at 20 cps. As shown in Fig. 2, a neutral beam was defined at 90° to the internal proton direction. A 4-ft tapered brass collimator produced a beam of one-foot-square cross section at the center of the apparatus, 20 ft from the target. The γ-ray component of the beam was attenuated with 8 radiation lengths (r.l.) of lead placed 1 ft from the target. Two dipole magnets with field integrals of 6×10^5 G cm each, placed before and after the collimator, swept charged particles out of the beam in a vertical plane. To minimize interactions of the beam particles, the first 14 ft of the beam path were evacuated, and at the apparatus the beam passed through a 10-ft long, 2-ft-diam helium-filled Mylar bag. This beam had an intensity of about 3×10^4 K_L/sec in the momentum range 150–450 MeV/c, with the spectrum peaked at 250 MeV/c. The neutron-to-K ratio was of the order of 1000 to 1, but few neutrons had energies above the π^0 production threshold.

[4] At the time of writing, the most recent review is by J. Steinberger, in Proceedings of the Topical Conference on Weak Interactions, Geneva, 1969, CERN Report No. 69-7 (unpublished).

[5] M. Banner, J. W. Cronin, J. K. Liu, and J. E. Pilcher, Phys. Rev. Letters **21**, 1107; **21**, 1103 (1968).

[6] An excellent review may be found in the article by T. D. Lee and C. S. Wu, Ann. Rev. Nucl. Sci. **16**, 511 (1966).

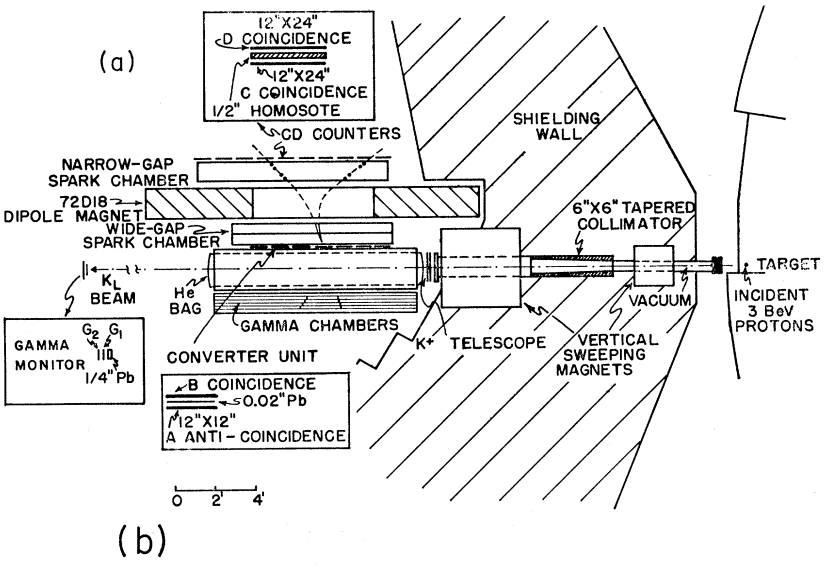

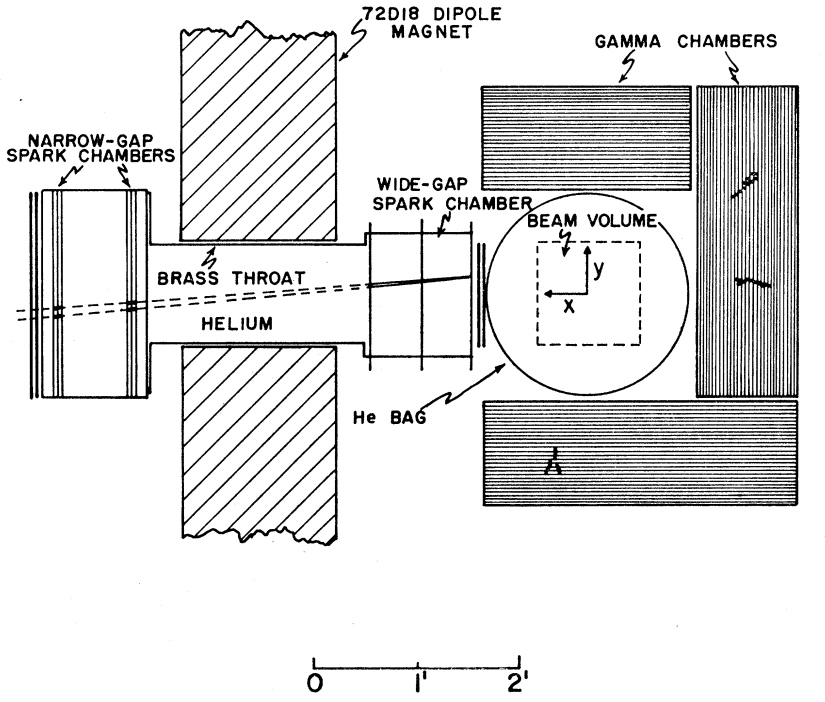

FIG. 2. (a) Top view of experimental apparatus. (b) Front view of experimental apparatus.

The experimental scheme was to measure accurately the direction and energy of one γ ray from K_L decay, and to observe the directions of the other decay products. The γ ray was converted in a 0.1-r.l. lead sheet and the resulting electron pair was momentum-analyzed in a magnetic spectrometer. The other decay products were detected in steel-plate spark chambers placed around the beam. In addition, the velocity of the decaying particle was measured by its time of flight from the target, using the fact that the internal protons struck the target in 1-nsec wide bunches every 67 nsec during the spill. The time at which each proton pulse hit the target was monitored by a Čerenkov counter placed 4 ft from the target at 20° to the proton beam direction.

As shown in Fig. 2, the spectrometer was built around a 72D18 magnet with a 12-in. gap and a central field of 2.1 kG ($\int Bdl = 1.4 \times 10^5$ G cm). Immediately after the conversion plane the directions of the electrons were determined in a two-cell wide-gap

spark chamber. The plates of the chamber were 1-mil aluminum foils placed 6 in. apart, and the cells were filled with a 90% neon, 10% helium mixture at room temperature and pressure. To reduce multiple scattering, the volume inside the magnet was filled with helium, contained by a brass throat. Helium was also used in a conventional four-gap spark chamber placed behind the magnet. The plates of this second chamber were also 1-mil aluminum foils, and the two pairs of $\frac{1}{2}$-in. gaps were separated by 8.5 in. The wide-gap spark chamber facilitated the correct pairing of the electron tracks entering and leaving the magnet, since it allowed observation of the track curvatures in the fringe field of the magnet. Thus the energy resolution of the apparatus was independent of multiple scattering in the lead converter.

A 5-ton array of steel-plate spark chambers (γ chambers) enclosed the three sides of the beam not covered by the spectrometer. The chambers below and beside the beam were 3 ft wide by 10 ft long, while the one above the beam was 2×10 ft. Each chamber consisted of three $\frac{1}{8}$-in. aluminum plates (0.17 r.l. total), followed by 20 $\frac{1}{8}$-in. stainless-steel plates (3.5 r.l. total).

Separate 35-mm cameras were used to photograph the spectrometer and γ chambers. The spectrometer was recorded in 90° stereo on a double 35-mm film frame. The γ chambers were viewed in narrow-angle stereo (approximately 10° at the center of the chambers) and were recorded on a single 35-mm film frame.

All the spark chambers were triggered when an electron-positron pair was detected in the spectrometer by scintillation counters. Four rows of counters were involved, as can be seen in Fig. 2(a). An event signal required a pulse from a single B counter behind the lead and no signal from its associated A counter in front of the lead. Signals were also required from two C counters and two D counters behind the magnet. An additional requirement was that the two C (and D) counters not be adjacent. Under normal running conditions with an 8-msec spill, this logic was satisfied about once every 12 sec. One trigger in five gave an event suitable for further analysis. This event yield (mainly 3π) was consistent with the calculated yield based on the estimated K_L flux in the 90° beam.

Two monitors were placed in the beam. The first was in position for only the last two-thirds of the experiment and was called the K^+ telescope. It was a pair of $10\times10\times\frac{1}{16}$-in. scintillation counters placed just before the decay region, and was used to monitor the presence of charged particles in the beam. The relative time between a spectrometer trigger and any coincidence in the K^+ telescope was recorded on the spectrometer film. The second monitor, called the γ monitor, was placed downstream from the apparatus. It consisted of a pair of $1\times1\times\frac{1}{4}$-in. scintillation counters behind a $\frac{1}{4}$-in. lead slab. These counters monitored the time of flight of direct γ rays from the internal target, thus checking the stability of the 67-nsec spill structure and the stabilty of the Čerenkov counter used to view the target.

For time-of-flight measurement, the beginning of the time interval was marked by a signal from the B counter responsible for the trigger, and the end by a signal from the on-target Čerenkov counter. The two timing signals were displayed on an oscilloscope and photographed. In addition, the spectrometer film also recorded the time of flight from a time-to-height, analog-to-digital converter combination. The two readout systems gave entirely consistent results.

The timing system was calibrated at the beginning and end of each week by measuring the time of flight of direct γ rays from the internal target to individual B counters. This data provided a reference point for each B counter. All times of flight referred to in this report are with respect to this γ-ray calibration point. The K^+ telescope was similarly calibrated with respect to each B counter.

Data were taken under a variety of operating conditions, as summarized in Table I. The data taken with a helium-filled beam volume under the operating conditions described above constitute the primary source of events for this study. These are referred to as the free-decay data.

Data were also taken with a 0.5-in. Hevimet regenerator (collision length = 3.1 in.) placed in the beam 9 in. upstream of the center of the apparatus, at $Z=-9$ in. Since the bulk of these events resulted from neutron interactions in the regenerator, they served to indicate the response of the apparatus to neutron-induced triggers. The regenerated K_S beam allowed the search for $K_S\rightarrow\gamma\gamma$. It was impossible to investigate other K_S decay modes because of the large flux of scattered neutrons entering the γ chambers during their sensitive time.

To estimate the effect of the helium in the decay volume, it was replaced with SF_6 gas for one week of data taking, and with air for a second week. To search for spectrometer triggers associated with shielding leaks the beam port was closed with 30 in. of lead and 4 in. of tungsten for a data-taking period of one week. The effect of anticounter inefficiency was investigated by turning the A anticounters off for several rolls of film. A one-week run was made with an $84\times12\times\frac{1}{2}$-in. piece of Lucite placed along the beam side of the anticounters. This Lucite was intended to serve as a target for charge exchange of π^- mesons from K_L decays. A background source from this process occurring in the first portion of the anticounters would have been greatly enhanced by the addition of the Lucite. Data were also taken with the high-voltage trigger to the γ chambers delayed by the period of the accelerator's synchrotron structure. The purpose of this run was to study the rate of accidental tracks in the γ chambers.

TABLE I. Spectrometer data.[a]

Condition of run	Beam monitor (10^6 counts)	No. of events	$P_\perp > 165$ MeV/c	TOF > 25 nsec	TOF > 25 nsec, $P_\perp < 165$ MeV/c
Helium	285.0	7305	629	3234	3086
SF_6	37.2	1749	372	523	456
Air	86.2	2144	225	900	837
Hevimet	49.7	4030	1356	989	733
Lucite	51.6	1702	147	728	689
Half field[b]	12.5	4509	21	1608	1600
Full field[b]	15.5	479	51	210	186
No anticounter	10.4	372	38	164	152
Port closed	82.3	18	5	7	5

[a] Data taken under adverse running conditions not included.
[b] These runs were made alternately at 1-h intervals, with helium in the beam volume.

An important calibration of the γ-chamber efficiency was made with cosmic rays at the start of each film roll, or approximately every 12 h. In addition, to confirm reconstruction calculatious, cosmic-ray data were taken with charged-particle tracks passing through all pairs of spark chambers, including the spectrometer chambers.

Normalization for most of the decay modes reported here is based upon the $K_L \to 3\pi$ events. The acceptance of the spectrometer for these decays is a strong function of the magnetic field of the spectrometer, and is estimated by a Monte Carlo computer simulation of the decay and detection processes. As one of several checks on the validity of the computed acceptance, data were taken with the magnetic field reduced to half the normal value.

III. FILM ANALYSIS

The spectrometer and time-of-flight data were first analyzed to obtain a set of events for which the momentum of one γ ray was accurately known. Subsets of these events were then selected as candidates for each decay mode, and the γ-chamber data for the subsets were then measured and analyzed to yield the final candidates.

A. Spectrometer Film

The spectrometer film was analyzed in a two-stage process. Each frame was first checked for a measurable electron pair. About one frame in five showed such a converted γ ray, and the scanners recorded a descriptive code for these events, together with their judgment of the correct pairing of the tracks in the top and side views of each chamber. The descriptive code recorded extra tracks, missing sparks, or very weak sparks. The pairing decision was based on individual spark quality but had little effect on the measured track momentum since most of the momentum information was contained in the top views. The results of this initial scan were passed to a second operator, who briefly checked the results and recorded with a film-plane digitizing machine the coordinates of two points in each view of the tracks before and after the magnet.

After track reconstruction, a series of checks was imposed on the data to ensure that the tracks seen entering and leaving the magnet were from the same particle, and that there was no appreciable scattering as they passed through the magnet. Tracks were rejected if they came within 0.5 in. of the brass throat inside the magnet aperture. This cut, together with a check that the two tracks had opposite curvature, eliminated 28% of the measured events. Three consistency checks on vertical-focusing effects and track continuity eliminated an additional 13%. No spectrometer data were retained where the gap efficiency of the γ chambers was lower than 90%. This requirement eliminated very few data.

In general, spectrometer data were scanned and measured only once. The scanning efficiency was 92%, and was the same for γ-ray energies above and below 165 MeV to within 3%. Because normalization for the branching ratios is internal, the absolute over-all spectrometer scanning efficiency is unimportant.

B. γ-Chamber Data

The γ-chamber data were measured twice by independent groups of physicists. The criteria for the selection of the γ-chamber data to be measured depended on the decay mode under consideration, and are discussed below in the section appropriate to each mode. The following general remarks are applicable to all decay modes.

The criterion for a measurable track was the presence of two or more contiguous sparks in both stereo views of a γ chamber. This criterion was chosen to maximize the detection efficiency, and minimize uncertainties in the calculation of these efficiencies. All tracks which originated in the first or second gaps of a γ chamber were referred to as charged particles, even though some of them were actual γ rays which converted in one of the first two aluminum plates. All other tracks were assumed to be γ rays. The modest measurement criterion requirement permitted a large number of sparks from neutron and K_L interactions in the beam volume to qualify as γ rays, with an accidental rate of about 25%. In addition, there was a 20% charged accidental rate

for short, two-gap recoil protons from n-p scattering. The probability of having two contiguous sparks from spurious breakdown in the chambers was observed to be negligible.

To record a track seen on the film, the positions of the first and last sparks of each track were measured in both stereo views. If the particle scattered or showered appreciably, the last spark position was taken to be that point along the initial direction of the track which was as close to the end of the track as possible. To facilitate the analysis, no more than four particles were measured in any given γ-chamber picture. When the number of tracks exceeded four, the shortest track was ignored, and in almost all cases, this was a two-spark charged particle. The actual number of events with more than four measurable tracks in the γ chamber was less than 5% of all the pictures examined.

IV. $K_L \rightarrow \pi^0\pi^0$ DECAY

A total of 7305 events remained after cuts were made for adverse running conditions. The transverse-momentum distribution for these events is shown in Fig. 3. Only the 629 events with the spectrometer γ ray having a transverse momentum $P_\perp$ greater than 165 MeV/c were analyzed for the $2\pi^0$ hypothesis. Although a selection of events based on an $E_{\text{c.m.}}$ above 165 MeV would have yielded a somewhat larger sample, the selection on transverse momentum was used as it is independent of the time-of-flight (TOF) measurement. The TOF measurement was expected to be in error by 67 nsec in about 2% of the events, because the spacing of the accelerated proton bunches limited the TOF measurement to modulo 67 nsec.

A. Event Fitting

1. Introduction

The γ ray detected in the spectrometer will be referred to as γ_4, and the γ ray associated with it to form the spectrometer π^0 will be called γ_3. The γ rays from the other π^0 will be referred to as γ_1 and γ_2. When all four γ rays from $2\pi^0$ decay were detected, the event was called a type-C event. When only two γ rays were observed in addition to γ_4, the event was classified type-A if these γ rays were γ_1 and γ_2, and as type-B if one of the two γ rays was γ_3.

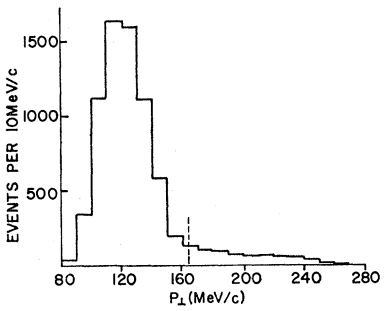

FIG. 3. Spectrometer γ-ray transverse momentum spectrum for free-decay data. The dashed line indicates the cut at $P_\perp = 165$ MeV/c.

All the particles observed in an event were assumed to be converted γ rays for the purpose of analysis, regardless of the gap in which the track originated. All events with two or more particles observed in the γ chambers were tested for the type-A hypothesis, using all possible combinations of two particles with γ_4. These events were also tested for type-B fits, using all possible combinations of two particles with γ_4, and letting each of the two associate with γ_4 in turn to form the spectrometer π^0. In addition, all events with three or more particles observed in the γ chambers were tested for the type-C hypothesis, using all possible combinations of three particles with γ_4, and pairing each of the three with γ_4 in turn. As will be discussed in Sec. V, an event may also be tested for the $K_L \rightarrow \gamma\gamma$ hypothesis.

The result of each attempt at a fit to a given hypothesis was recorded on magnetic tape, and a selection program was used to choose the most likely fit, according to the following priority list: (1) type C, (2) type A or type B, (3) $\gamma\gamma$, and (4) no fit. When there was more than one fit in any particular class, the selection program followed certain rules which will be described shortly. Any one or more of the different kinds of fits could be suppressed in the selection procedure in order to study the effect on the other types of fits.

The basic procedure for each type of fit was the same, except for the obvious differences in kinematic details. Because of the relatively low momentum of the K_L mesons (100–500 MeV/c), the energies of the γ rays were rather low (10–400 MeV in the laboratory); consequently, the directional information contained in their tracks was poor. On the other hand, the spectrometer had been designed to yield good directional information for its observed γ ray, the average angular uncertainty in its direction being 2.5°. Therefore, the fitting scheme made use of the conversion point and direction of γ_4, but only the conversion points of the other γ rays observed in the steel-plate chambers.

In order to find a best-fit decay vertex, a search was conducted along the trajectory of γ_4 across the beam volume for that point at which the fit to a given hypothesis was best. Specifically, the trial for a certain hypothesis involved fits at hypothetical decay points taken at 0.5-in. intervals across the beam, along the trajectory of γ_4, with the restriction that these points be no more than 2 in. outside the physical limits of the beam region. At each hypothetical decay point, the directions of the other particles observed in the γ chambers were constructed by joining this hypothetical decay point to their conversion points in the chambers, and the event was transformed to the c.m. system of the decaying particle, with the use of its measured TOF.

The kinematic fits for type-A, -B, and -C events

will now be described, along with the restrictions specified by the selection program for each class of fit. The vector $\hat{u}_i$ will be used to denote the unit directional vector of the ith γ ray in the c.m. system of the decaying particle, and p_i will represent its c.m. momentum. The measured c.m. momentum of the spectrometer γ ray is p_4 ($=E_{\text{c.m.}}$). In the fitting procedure, p_4 was increased by 4% to compensate for bremsstrahlung and ionization losses; this adjusted value will be denoted by $\tilde{p}_4$.

2. Type C

The type-C fit will be discussed first since it involves all four γ rays from $K_L \to 2\pi^0$ decay, and is the most desirable class of fit. In principle, if the decay vertex were known, the type-C fit would be a three-constraint fit. The unknowns would be the energies of the three γ rays observed in the γ chambers, while the conservation of four-momentum and the requirement that the K_L decayed into two π^0's yield six equations. However, since a search is conducted for a best-fit decay point along a segment of a line, one constraint is partially lost, and the C fit can be considered a two-constraint fit.

At each hypothetical decay point along the trajectory of γ_4, momentum conservation in the c.m. system requires that

$$p_1\hat{u}_1+p_2\hat{u}_2+p_3\hat{u}_3+p_4\hat{u}_4=0. \tag{4}$$

This set of three simultaneous equations can be solved to give

$$p_i=\lambda_i p_4, \quad i=1, 3. \tag{5}$$

The parameters λ_i depend only on the directions of the γ rays and are independent of p_4. The mass of the decaying particle is given by energy balance,

$$m^*=\sum_{i=1}^{4} p_i$$

$$=p_4(1+\lambda_1+\lambda_2+\lambda_3), \tag{6}$$

and the associated masses of the decay particles are

$$m_{12}=p_4[2\lambda_1\lambda_2(1-\hat{u}_1\cdot\hat{u}_2)]^{1/2} \tag{7}$$

and

$$m_{34}=p_4[2\lambda_3(1-\hat{u}_3\cdot\hat{u}_4)]^{1/2}. \tag{8}$$

A fitting statistic χ^2 is formed using the mass ratios m_{12}/m^* and m_{34}/m^*, both of which are independent of p_4:

$$\chi^2=\left[\left(\frac{m_{12}}{m^*}-\frac{m_\pi}{m_K}\right)^2+\left(\frac{m_{34}}{m^*}-\frac{m_\pi}{m_K}\right)^2\right]\left(\frac{\sigma_\pi}{m_K}\right)^{-2}, \tag{9}$$

where m_π, m_K denote the π^0 and K_L masses, respectively, and $\sigma_\pi=10$ MeV is a measure of the expected resolution in m_{12} and m_{34}. This particular choice of χ^2 does not involve the measured momentum p_4, and no assumptions have been made about the identities of the particles with masses m^*, m_{12}, and m_{34}. The χ^2 is merely a measure of how close the mass ratios m_{12}/m^* and m_{34}/m^* are to the expected ratio m_π/m_K. It should be pointed out that the transformation to the c.m. system of the decaying particle requires only knowledge of its velocity and not its mass.

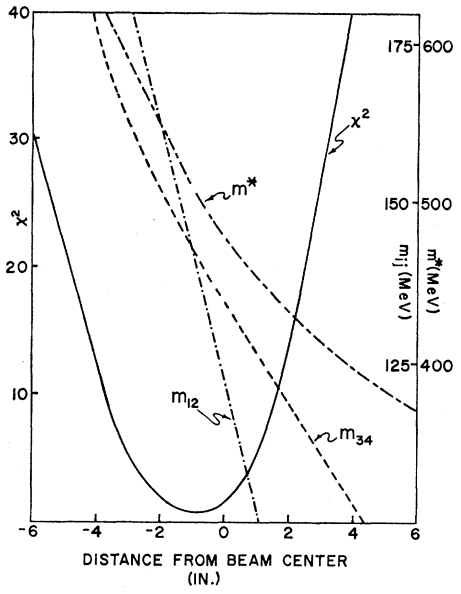

FIG. 4. Kinematic fit across face of beam for a type-C event.

Figure 4 shows the variations in χ^2, m^*, m_{12}, and m_{34} across the face of the beam for a typical type-C event. For each attempt at a C fit, the best value of χ^2 across the beam is kept, and the values of m^*, m_{12}, and m_{34} calculated at the corresponding decay point, using Eqs. (6)–(8), but with $\tilde{p}_4$ in place of p_4. In addition, the cosine of the opening angle between γ_1 and γ_2 in the center-of-mass system, $\hat{u}_1\cdot\hat{u}_2$, is also calculated.

The final C fit selected was the one with the lowest χ^2, subject to the conditions $\chi^2<9$, and $350\leq m^*\leq 650$ MeV. In addition, the selection program required that a good type-C fit have no more than one γ ray converting in the first two aluminum plates of a γ chamber, and that $\tilde{p}_4<240$ MeV. Events with two or more γ rays appearing as charged particles in the γ chambers are expected to be less than 1% of all true C events. Results of the type-C fit are given in Sec. IV A 6.

3. Type A

The type-A fit involves only two γ rays besides γ_4, and is thus not as restrictive as the type-C fit. However, both γ rays from the other π^0 are used directly in the A fit, making it more restrictive than the type-B fit, in which only one γ ray from the other π^0 is used directly.

By searching along the line of the spectrometer γ ray for a best-fit decay point, the type-A fit becomes essentially a zero-constraint fit since the direction of γ_3 is now unknown. However, it must be emphasized that the search is conducted only along a segment of

this line, and not over all space, since a true decay point must necessarily lie within the beam volume.

The type-A fit assumes that a K_L decayed into two neutral pions. At each hypothetical decay point, the following relations express energy and momentum balance in the K_L c.m. system:

$$E_\pi = p_1 + p_2 = \tfrac{1}{2} m_K , \tag{10}$$

$$p_\pi^2 = E_\pi^2 - m_\pi^2 , \tag{11}$$

$$p_\pi^2 = p_1^2 + p_2^2 + 2 p_1 p_2 \hat{u}_1 \cdot \hat{u}_2 , \tag{12}$$

$$p_\pi \hat{u}_\pi = p_1 \hat{u}_1 + p_2 \hat{u}_2 , \tag{13}$$

where E_π and p_π denote the energy and momentum of the other π^0, and $\hat{u}_\pi$ its direction in the K_L c.m. system. The maximum value of $\hat{u}_1 \cdot \hat{u}_2$ is 0.412 for a true event. However, values of $\hat{u}_1 \cdot \hat{u}_2 \leq 0.5$ at any given hypothetical decay point are accepted, with the value of $\hat{u}_1 \cdot \hat{u}_2$ set at 0.412 if it exceeded this value. This corresponds to a reconstructed opening angle 6° smaller than the minimum c.m. opening angle. From Eqs. (10) through (13), the two possible directions of the other π^0 can be found. The ambiguity exists because it has not been specified if $p_1 > p_2$, or vice versa.

The direction of the spectrometer π^0 is $-\hat{u}_\pi$. The energy of the spectrometer γ ray p_4 can then be predicated from the relationship

$$\tilde{p}_4 = \gamma_\pi p_4 (1 + \beta_\pi \hat{u}_\pi \cdot \hat{u}_4) , \tag{14}$$

where $\tilde{p}_4 = \frac{1}{2} m_\pi$ represents the momentum of γ_4 in the c.m. system of the spectrometer π^0, and γ_π and β_π can be computed with the values of E_π and p_π. The predicted value of p_4 is then compared with the measured value $\tilde{p}_4$ to check the closeness of the fit.

Figure 5 shows the variation in p_4 and $\hat{u}_1 \cdot \hat{u}_2$ across the face of the beam for a typical type-A fit. For each

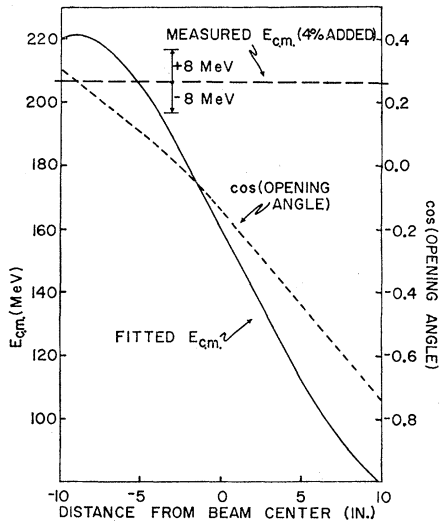

FIG. 5. Kinetic fit across face of beam for a type-A event. The measured $E_{c.m.}$ is increased by 4% to compensate for bremsstrahlung and ionization losses.

attempt at an A fit, the predicted value of p_4 that is closest to $\tilde{p}_4$ is kept, provided that $|p_4 - \tilde{p}_4| < 8$ MeV and $\tilde{p}_4 < 240$ MeV. The quantity $\hat{u}_1 \cdot \hat{u}_2$ is calculated so that its distribution can be compared with the expected distribution for π^0 decay.

The selection program required a good A fit to have no more than one γ ray appear as a charged particle, and this charged particle must not have a spark in the first gap of a γ chamber. From cosmic-ray calibrations, approximately 95% of all true charged particles left a spark in a first gap. For each attempted A fit, the direction and energy of the missing γ ray γ_3 was computed, as well as the probability that it converted in the γ chamber. Multiple A fits were possible for those events which had one or more accidental tracks. The solution with the minimum probability of converting γ_3 was retained. Results for the type-A fits are presented in Sec. IV A 6.

4. *Type B*

Although the type-B events involve two γ rays detected in the γ chambers in addition to the spectrometer γ ray γ_4, the only possible kinematic fitting procedure uses only one of these γ rays to test if it could combine with γ_4 to form a π^0 from a $2\pi^0$ decay. Because the information contained in the other γ ray detected in the γ chambers is not used in the fitting procedure, and because the decay vertex is not known, the B fits are susceptible to background contamination, and it was decided to exclude them altogether. The elimination of type-B fits left the selection program with the choice of type-C, type-A, $\gamma\gamma$, and no-fit events, in that order of priority. The no-fit events were those in which the selection program found no suitable A, C, or $\gamma\gamma$ fits among all the attempts at a fit for a given event.

5. *Remeasurement*

The two independent measurements of the γ-chamber film were analyzed separately, using the same information from the corresponding spectrometer measurements. The analysis tapes for these measurements were then read by the selection program, and the resultant lists of fits for A, C, and $\gamma\gamma$ events were compared. Events which were clearly $K_L \rightarrow \gamma\gamma$ on both lists were removed from further consideration. Events which were type-C on both lists were noted, and the measurement with the lower value of χ^2 was retained. Those which were type-A on both lists were also noted, and the decision on which of the two measurements was to be kept was made with the toss of a coin. Those events whose two measurements disagreed with one another were measured a third time. That earlier measurement which agreed with this third measurement was kept, and the above procedure of selecting the better fit was repeated.

The first measurement of the γ-chamber film resulted in 29 C events and 35 A events, whereas the second

gave 31 C events and 33 A events. The total number of A+C events observed in each measurement was thus 64. The final tabulation, made from a combination of the three measurements, showed 39 type-C fits and 26 type-A fits, giving a total of 65 (A+C) events. Thus, although the scanning efficiency in each measurement for type-C events was about 75%, the scanning efficiency for A+C events was practically 100%. This reflects the fact that γ_3 is a low-energy γ ray and could easily be overlooked in the γ-chamber film for a type-C event, with the result that the event would be classified as a type-A fit. However, there is no serious consequence on the final result, since the value of $|\eta_{00}|$ will be calculated from the total number of A+C events observed.

Remeasurement of the spectrometer film for the final group of 65 (A+C) events showed that the values of $P_\perp$ and $E_{\text{c.m.}}$ for each of these events were reproducible within the measurement error, which was about 2.8% full width at half-maximum (FWHM), and in no event was a serious discrepancy found.

6. Results for A and C Events

The χ^2 distribution for the type-C candidates and the resulting m^* distribution for the events with $\chi^2<9$ is shown in Fig. 6. There were three events with m^* outside of the acceptable range, $350\leq m^*\leq 650$ MeV, leaving a final total of 39 type-C events. Figure 7 shows the distribution in m_{12} and m_{34}.

The final tabulation showed 26 type-A events; the distribution in $\hat{u}_1\cdot\hat{u}_2$ for these events is shown in Fig. 8(b). It should be noted that the type-A distribution in $\hat{u}_1\cdot\hat{u}_2$ is somewhat broader than the corresponding distribution for the type-C events, as shown in Fig. 8(a). This arises from the exclusion of the type-B fits, with the result that approximately 20% of the type-A fits were really made with type-B events.

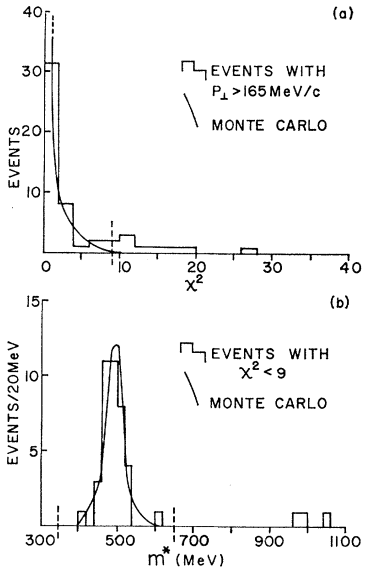

FIG. 6. Results for the type-C hypothesis. (a) The χ^2 distribution. Only events with $\chi^2<9$ are kept. (b) The reconstructed decay particle mass m^* for all type-C fits with $\chi^2<9$. The mass peak is centered at 490 MeV, with a FWHM of 60 MeV. A total of 39 events lie within the fiducial region $350\leq m^*\leq 650$ MeV.

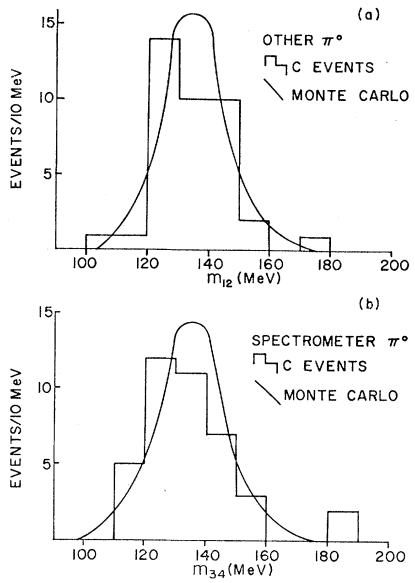

FIG. 7. (a) Reconstructed mass for the other π^0, m_{12}. (b) Reconstructed mass for the spectrometer π^0, m_{34}. Both distributions are centered at 135 MeV, each with a FWHM of 30 MeV.

7. Checks for A and C Events

The Monte Carlo calculations, described fully in Sec. IV C, predict various distributions for the A and C

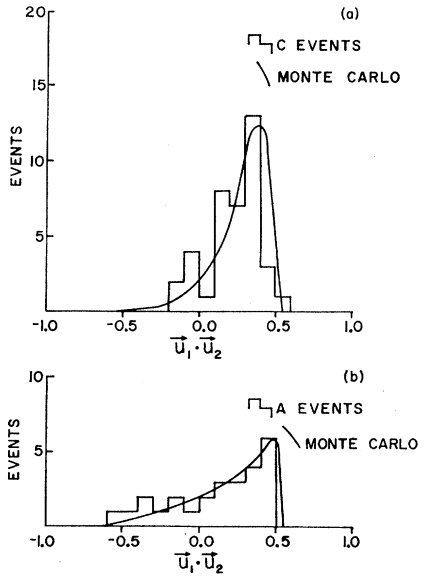

FIG. 8. Opening-angle distributions for γ rays from the other π^0. (a) $\hat{u}\cdot\hat{u}_2$ for 39 type-C events. (b) $\hat{u}_1\cdot\hat{u}_2$ for 26 type-A events.

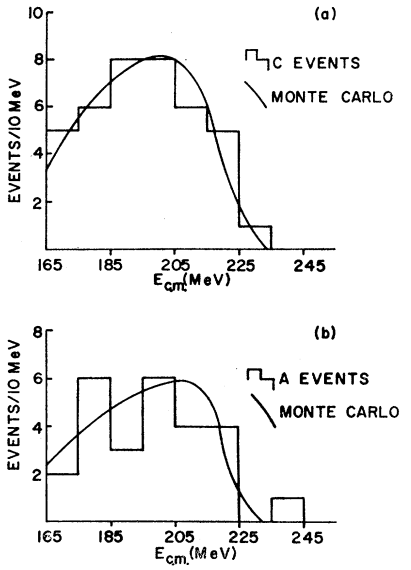

FIG. 9. Energy distribution of spectrometer γ ray in the K_L c.m. system for $2\pi^0$ events. (a) $E_{c.m.}$ distribution for 39 type-C events. (b) $E_{c.m.}$ distribution for 26 type-A events.

events which can be checked against the corresponding experimental distributions. A few of the more significant comparisons will now be presented.

A total of 13 type-C events had one γ ray appearing as a charged particle in the γ chambers; 10 were expected. This latter number included the probability for Dalitz pairs in the decay of a π^0. A total of four type-A events had a γ ray converting in the second aluminum plate of a γ chamber, while two were expected from Monte Carlo studies.

A survey of the film for the 65 (A+C) events showed that 48% of the group had one or more accidental tracks in the γ chambers, while the accidental survey indicated that this number should have been around 50%.

The distribution in the c.m. energy $E_{c.m.}$ of the spectrometer γ ray is shown in Fig. 9 for the A+C events. The predicted lab energy spectrum for the γ rays observed in the γ chambers for the type-C events was calculated from Eq. (5) and is shown in Fig. 10. The distribution in the cosine of the angle of incidence of γ rays on the γ-chamber plates is shown in Fig. 11. In each case, the agreement with the expected distribution is good. Figure 12 shows the relationship between the predicted lab energy of a γ ray and the mean number of sparks observed in the γ chambers. The average energy per spark is indicated to be $\sim$25 MeV for γ rays with the incident angle distribution shown in Fig. 11.

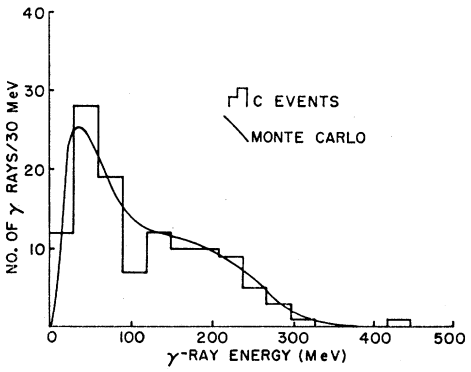

FIG. 10. Distribution in lab energies of γ rays observed in γ chambers for type-C events.

B. Background Studies

In this section, the several possible contributions to background contamination in the sample of A+C events will be discussed.

1. Beam Interactions

A run was made with the heavy gas SF_6 in the beam volume instead of helium. This had the effect of increasing the neutron and K_L interaction rates in the beam volume, as well as increasing the rate of accidental tracks in the γ chambers. A total of 372 events were observed to have $P_\perp > 165$ MeV/c, and a total of seven type-C and 12 type-A events were found for the SF_6 run. Figure 13 shows the relevant distributions for the SF_6 (A+C) events. Instead of treating each category separately, the combined category of A+C shall be used to compare the SF_6 data with the helium data since there are so few events.

The length of the SF_6 run was 7.0$\pm$0.5 times shorter than the length of the helium run for the data presented here. Hence, 9$\pm$3 true A+C events may be expected from the K_L decays during the SF_6 run, leaving an excess of 10$\pm$3 (A+C) events in the SF_6 run which were due to interaction background. The neutron interaction rate in SF_6 has been estimated to be 14 times that in helium,[7] and the study of the no-fit events in the SF_6 and helium runs indicated that this

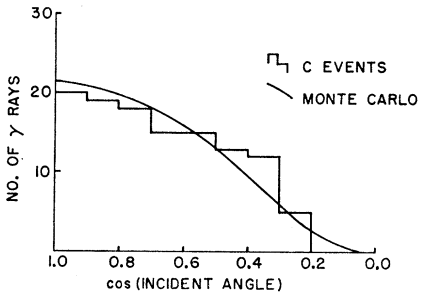

FIG. 11. Distribution in cosine of angle between incident γ-ray direction and the normal to a γ-chamber plate. The γ-ray direction is constructed with its conversion point and the best-fit decay vertex.

[7] B. Margolis, Nucl. Phys. **B4**, 433 (1968).

ratio was 11.9±3.0. Hence, with the factor of 7 in the relative lengths of running times, the SF_6 run indicated that a total of 6±4 interaction background events may be expected in the helium A+C total if the excess of A+C events in the SF_6 run were taken to be purely from interactions, including the possibility of K_S regeneration. The three events observed in the helium run with $\chi^2<9$ but $m^*>650$ MeV, if treated as interaction background events, would predict 5±2 similar events for the SF_6 run. A total of four such events was indeed observed in the SF_6 run.

2. $3\pi^0$ Background

The following study of $3\pi^0$ events was made to determine the background in the sample of $2\pi^0$ events had there been some drastic resolution failure in the spectrometer, causing $3\pi^0$ events to spill over into the $P_\perp>165$-MeV/c region.

First of all, in order to appreciate the $3\pi^0$ background problem which would have been present had there not been a cut of $P_\perp=165$ MeV/c, approximately 15% of the events in the 3π region $P_\perp<165$ MeV/c, were fully measured for particles in the γ chambers. The 927 such events were then analyzed with the $2\pi^0$ analysis program, and there were 211 events in which a combination of four particles gave a $\chi^2<9$, with one of the four always being the spectrometer γ ray. The χ^2 and m^* distributions for these events are shown in Fig. 14. There were 49 events in the type-C fiducial region, $350\leq m^*\leq 650$ MeV, but the peak in m^* was at 350 MeV instead of m_K. Thus if all the available data had been analyzed without the $P_\perp>165$-MeV/c cut, the true $2\pi^0$ mass peak would be masked by the $3\pi^0$ m^* distribution, since the $2\pi^0$ events would then constitute only ~17% of all events in the $350\leq m^*\leq 650$-MeV region, even with the bias in the spectrometer efficiency favoring γ rays from $2\pi^0$ decays.

Figure 15 shows that the observed $E_{\text{c.m.}}$ distribution agrees very well with the expected distribution, indicating that the spectrometer resolution was well understood. Even stronger evidence is provided by the study of the $K_L \to \gamma\gamma$ decay mode, as will be discussed in Sec. V. However, in order to examine just how the $3\pi^0$ events could have contaminated the experimental results had there been a resolution failure in the spectrometer, the sample of fully measured $3\pi^0$ data was analyzed with the value of $E_{\text{c.m.}}$ $(=p_4)$ for each event placed arbitrarily in the range $165<E_{\text{c.m.}}<230$ MeV. This particular operation was given the title

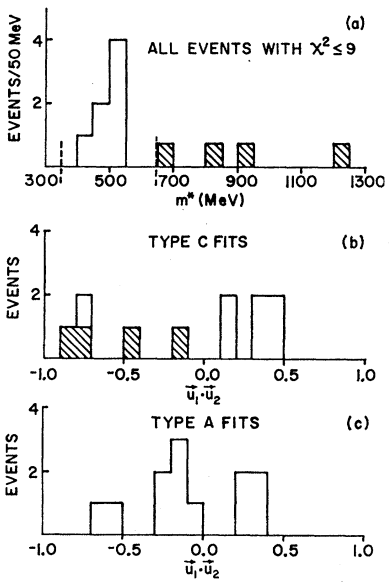

FIG. 13. $2\pi^0$ candidates for the SF_6 data. (a) m^* distribution for type-C fits with $\chi^2<9$. The shaded events with $m^*>650$ MeV are not accepted. (b) Distribution in $\hat{u}_1\cdot\hat{u}_2$ for the type-C fits. The shaded events correspond to the C fits with $m^*>650$ MeV, and are not accepted. (c) Distribution in $\hat{u}_1\cdot\hat{u}_2$ for the type-A fits.

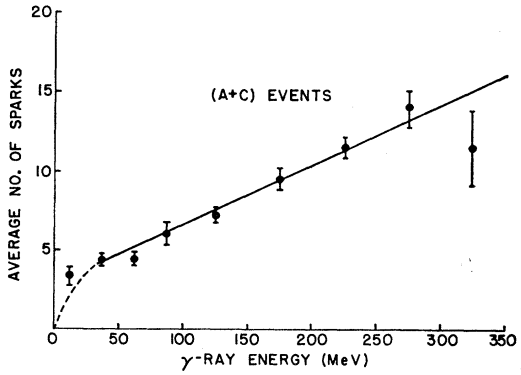

FIG. 12. Plot of average number of sparks in a γ-ray track versus the γ-ray energy for the A+C events.

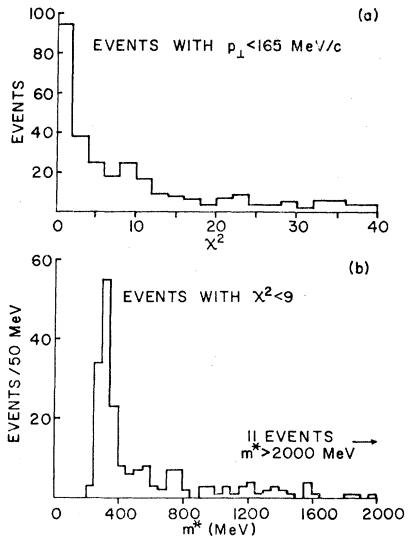

FIG. 14. Results for type-C fits with events in the 3π region, $P_\perp<165$ MeV/c. (a) The χ^2 distribution. (b) The m^* distribution for all events with $\chi^2<9$. The mass peak is centered at 350 MeV.

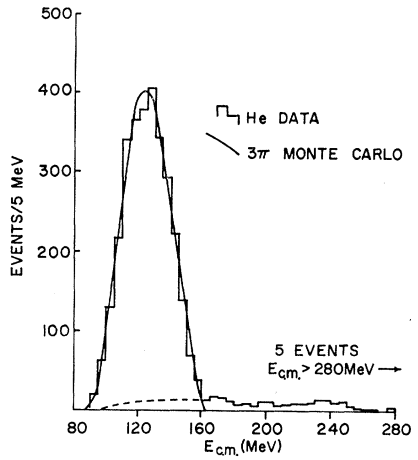

FIG. 15. $E_{\text{c.m.}}$ spectrum for all events with TOF>25 nsec. These events are expected to be free of neutron interaction background. The dashed distribution is the estimated contribution from $2\pi^0$, $\gamma\gamma$, and other background events in the 3π region, $E_{\text{c.m.}}<165$ MeV.

"$E_{\text{c.m.}}$-raised." Figure 16 shows the resulting m^* distributions for these $E_{\text{c.m.}}$-raised events when analyzed for type-C fits. The position of the m^* peak is centered about the K mass, but there is a tail which is absent from the m^* plot for the true type-C events, as shown in Fig. 6(b). The $E_{\text{c.m.}}$-raised m^* distribution is now used as a guide to evaluate the number of $3\pi^0$ events in the experiment which spilled past $P_\perp=165$ MeV/c because of a resolution failure in the spectrometer, and were analyzed as type-C fits. The ratio of events in the tail ($m^*>650$ MeV) to those in the type-C fiducial region ($350\leq m^*\leq 650$ MeV) for the $E_{\text{c.m.}}$-raised events indicates that three observed events, with $m^*>650$ MeV and $P_\perp>165$ MeV/c, would correspond to 3.5 possible $3\pi^0$ background events among the 39 type-C fits. However, since the three events with $m^*>650$ MeV and $P_\perp>165$ MeV/c are consistent with pure interaction background as determined in the SF_6 run, and since there is no evidence for any serious resolution failure in the spectrometer, no subtraction was made for $3\pi^0$ background resulting from resolution failure.

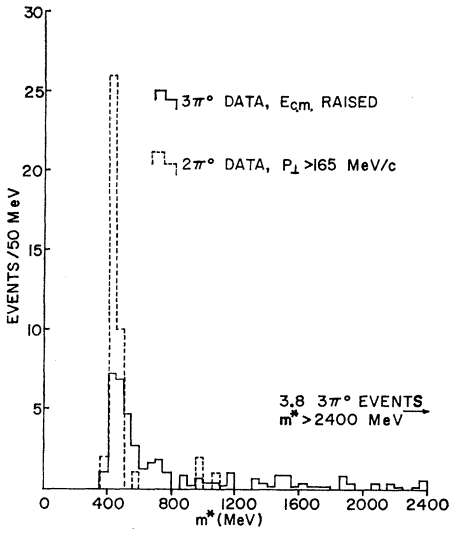

FIG. 16. The m^* distribution for type-C fits made with the events in the $3\pi^0$ region, $P_\perp<165$ MeV/c, but with the $E_{\text{c.m.}}$-raised resolution. The distribution is normalized to the 39 true type-C events observed in the $2\pi^0$ region, $P_\perp>165$ MeV/c, whose m^* distribution is shown as the dashed plot.

3. *Off-Axis K_L's*

There are two processes which lead to a component of off-axis K_L's in the beam, namely, elastic scattering off the last sweeping magnet, and elastic scattering off helium in the decay volume. With a K_L off axis, there is the possibility that a γ ray from its decay into $3\pi^0$ will have a $P_\perp>165$ MeV/c, resulting in a potential source of background in the $2\pi^0$ events.

The average angle for K_L's which scatter off the sides of the last sweeping magnet and enter the decay volume is $\sim 20°$. However, since these K_L's are off-axis, they would have to decay within the first 3 or 4 ft after leaving the sweeping magnet in order to have decayed within the decay volume. Thus, the off-axis K_L decays may be expected to appear as an excess of spectrometer events in the upstream region, $Z<-25$ in. The distribution in Z for the conversion points in the thin Pb converter for all the observed spectrometer γ rays is shown in Fig. 17, and a comparison with the expected distribution shows a deficiency of 1% for events with $Z<-25$ in. An upper limit of 1% is placed on the fraction of events observed in the spectrometer which were due to K_L's that scattered off the last sweeping magnet.

A Monte Carlo study, similar to that described in Sec. IV C, for K_L's at 20° off axis indicates that less than 5% of the detected 3π γ rays will have a $P_\perp>165$ MeV/c, and that of these, about one in three would fit a type-A or -C event. Thus, normalized to the ~ 6000 observed 3π spectrometer events with $P_\perp<165$ MeV/c, as discussed in Sec. IV D, a maximum of 1 ± 1 background A+C events may be expected from K_L's which scattered off the last sweeping magnet.

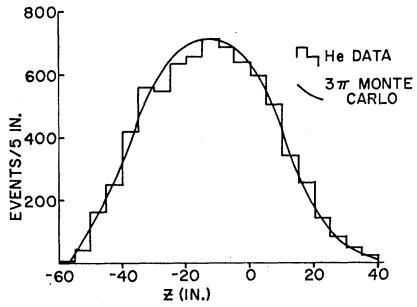

FIG. 17. Distribution in Z of decay point for all events observed in the helium run. The apparatus was centered about $Z=0$.

Similar calculations indicate that no contamination is expected from off-axis K_L's resulting from the elastic scattering of K_L off helium.

4. *Background from Type-B Events*

When an accidental track was added to a type-B event, it was found that 20% of these events would be analyzed as type-C fits. With the established rates of accidental tracks in the γ chambers, and with the known observed ratio of A, B, and C events, 1 ± 1 events in the final sample of C fits may be expected to be type-B with the presence of an additional accidental track. The problem of B's or C's fitting as A's, and the problem of A's transforming to C's with the presence of accidental tracks, will be taken into account in the final calculation of the A and C detection efficiencies, as described in Sec. IV C.

5. *No-Fit Events*

There remains to be examined a group of some 440 events which contained a spectrometer γ ray with $P_\perp > 165$ MeV/c, but which either left no tracks in the γ chambers, or failed to fit the $2\pi^0$ or $\gamma\gamma$ hypotheses. These are the no-fit events. Included in this total one expects approximately 55 genuine $2\pi^0$ and $\gamma\gamma$ events which failed to pass the kinematic fits, or which had too many γ rays unconverted in the γ chambers. A full understanding of the source of the other no-fit events is excluded by a lack of statistics, and by a general lack of information about these events.

The TOF distribution of the no-fit events is given in Fig. 18(a). The distribution for $2\pi^0$ and $\gamma\gamma$ events is plotted in Fig. 18(b). The no-fit event distribution shows a peak at very short times of fluight, where π^0 production by neutrons on helium is possible. Kinematically, only neutrons with TOF < 25 nsec were above the threshold for single-π^0 prduction on helium and could give rise to γ rays with $P_\perp > 165$ MeV/c. It is estimated that half of the no-fit events are from this source. The remainder of the no-fit events appear to be induced by the K_L beam, either by interaction of K_L in the helium, or by decay processes such as $K_L \to \pi e \nu$ giving apparent γ rays in the spectrometer with a small but non-negligible probability. A detailed study of these processes has been made in a separate unpublished report.[8] It is shown there that a qualitative understanding of the no-fit events is possible with the help of data collected during the SF_6 run, the port-closed run, the no-anti run, and the Lucite run.

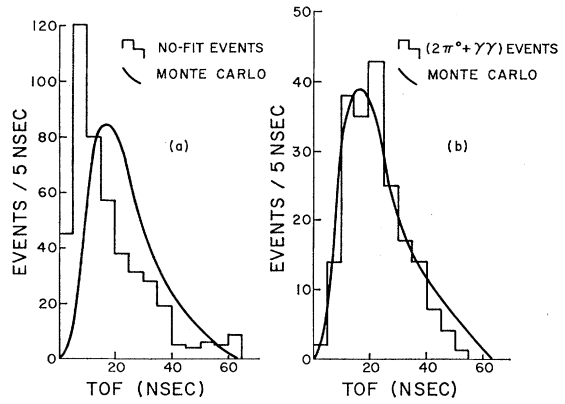

FIG. 18. (a) TOF distribution for the no-fit events observed in the helium run. (b) TOF distribution for the A+C events and $\gamma\gamma$ events. The Monte Carlo curve is obtained from the TOF distributions for simulated $2\pi^0$ and $\gamma\gamma$ events for both (a) and (b).

6. *Summary*

In summary, the background subtractions that must be made from the observed sample of 65 (A+C) events are the following:

6 ± 4 for interaction background,

1 ± 1 for off-axis K_L background, and

1 ± 1 for type B fitting as type C with the presence of accidental tracks.

The number of observed type-(A+C) $2\pi^0$ events with a spectrometer γ ray having $P_\perp > 165$ MeV/c is thus

$$N_{AC} = 57\pm9, \qquad (15$$

where the error is statistical.

C. Efficiency Calculations

In this experiment, the normalization for the number of $2\pi^0$ events found in Sec. IV B was made with the known decay rate $\Gamma(K_L \to 3\pi^0)$. This procedure involved two distinct efficiency calculations. First we calculated the relative efficiency to detect in the spectrometer single γ rays from $3\pi^0$, $\pi^+\pi^-\pi^0$, and $2\pi^0$ decays. Secondly, given a detected $2\pi^0$ γ ray, we calculated the probability that two or three associated γ rays would convert in the γ chamber and, in addition, fit as either a type-A or type-C event using the procedures discussed in Sec. IV A. Similar efficiency calculations were made for the other decay modes studied. All the efficiency calculations made use of the Monte Carlo technique.

1. *Spectrometer-Efficiency Calculations*

The input data for the spectrometer-efficiency calculations included the momentum spectrum of the K_L beam, the energy and angular distributions of single γ rays from the appropriate K_L decay mode in its center of mass, the magnetic field integral for the spectrometer magnet, and the geometry of the apparatus. Careful consideration was also given to the problems of bremsstrahlung and ionization energy loss, the sharing of the γ-ray energy between the electron and positron, multiple scattering, vertical focusing, and the exponential decay of the K_L. Since the $2\pi^0$

[8] J. K. Liu, thesis, Princeton University, 1968, Elementary Particles Laboratory Report No. 48 (unpublished).

TABLE II. Spectrometer efficiency calculations.

	$3\pi^0$	$\pi^+\pi^-\pi^0$	$2\pi^0$	$\gamma\gamma$	$\pi^0\gamma\gamma$
$10^3\times$raw efficiency[a]	1.099	0.607	12.04	50.02	9.950
Angular efficiency correction	0.930	0.930	0.808	0.780	0.854
$10^3\times$final efficiency ϵ[b]	1.022±0.051	0.565±0.028	9.730±0.485	39.00±2.00	8.490±0.420

[a] These efficiencies are only relative and do not represent absolute efficiencies.
[b] Errors of ±5% have been quoted.

decays are normalized to the $3\pi^0$ decays observed in the experiment, only relative spectrometer efficiencies were computed. The cuts which were applied to the Monte Carlo events were identical with those used for the experimentally observed events.

The results for the relative spectrometer efficiencies for the $3\pi^0$, $\pi^+\pi^-\pi^0$, $2\pi^0$, and $\gamma\gamma$ decay modes are shown in Table II. The angular-efficiency correction factor represents a correction for the inefficiency of the wide-gap spark chamber for tracks at large angles to its normal, and was obtained by a comparison of experimental and Monte Carlo angular distributions for electron pairs observed in the wide-gap chamber.

It was important to confirm the spectrometer efficiency calculations experimentally, since the final computation of the branching ratio $\Gamma(K_L\to 2\pi^0)/\Gamma(K_L\to 3\pi^0)$ depends on the efficiencies for normalization. The method chosen for this experimental check was to run with the spectrometer at half the normal magnetic field. Accordingly, the experiment was run with the magnet at full and half-field alternately, each run lasting approximately 1 h.

The half-field $E_{\text{c.m.}}$ distribution is shown in Fig. 19, and the agreement with the expected distribution is very good. The relative efficiency of the spectrometer for single γ rays from the 3π decay modes for the full-field and half-field runs was found experimentally to be

$$(\epsilon_{3\pi})_{\text{half}}/(\epsilon_{3\pi})_{\text{full}}=11.0\pm0.7 \quad \text{(expt)}. \qquad (16)$$

This is to be compared with the predicted ratio,

$$(\epsilon_{3\pi})_{\text{half}}/(\epsilon_{3\pi})_{\text{full}}=11.5\pm1.5 \quad \text{(Monte Carlo)}, \qquad (17)$$

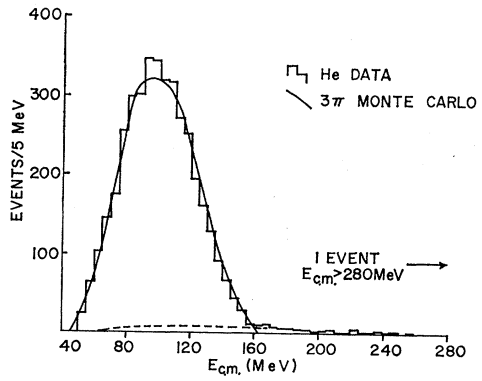

FIG. 19. The $E_{\text{c.m.}}$ spectrum for γ rays observed in the spectrometer during the half-field run. The dashed curve is the expected contribution from $2\pi^0$, $\gamma\gamma$, and interaction background events in the 3π region, $E_{\text{c.m.}}<165$ MeV.

where the error is mostly due to an uncertainty in the correction for multiple scattering of the electrons in the Pb converter, scintillation counters, spark-chamber foils, and neon gas. This uncertainty is only significant at half-field, where the acceptable electron energies can be as low as 20 MeV in the laboratory. The corresponding lower limit is 50 MeV for the full-field run.

The computed spectrometer efficiencies have been checked for sensitivity to the input parameters. From Fig. 20 it is seen that the predicted TOF spectrum does not quite fit the observed spectrum. If the Monte Carlo TOF spectrum is modified to fit the data, the largest change is a 3% shift in the efficiency ratio for $\Gamma(K_L\to\gamma\gamma)/\Gamma(K_L\to 3\pi)$. In addition, a ±3% uncertainty for this efficiency ratio arises from the ±0.5% uncertainty in the mapping of the magnetic field. Taking these facts into account, we have assigned a standard deviation of 5% for each calculated spectrometer efficiency.

2. γ-Chamber Efficiency Calculations

Monte Carlo $2\pi^0$ decays were generated in the γ chambers for those Monte Carlo spectrometer events where the observed $P_\perp$ of the detected spectrometer γ ray was greater than 165 MeV/c. These events were then analyzed in order to determine the detection efficiency for A and C events, ϵ_{AC}. The detection of a γ ray in the γ chambers involved three factors: (1) the geometrical detection, representing the fact that the γ ray passed through the spark-chamber material, (2) the conversion probability, indicating the likelihood that the γ ray produced a charged particle, and (3)

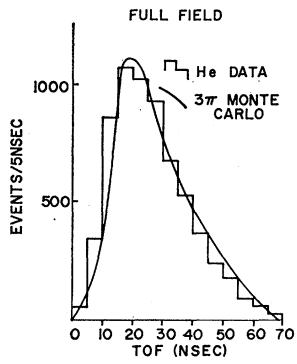

FIG. 20. TOF distribution for all events observed in the helium run.

TABLE III. $2\pi^0$ detection efficiency.[a]

Condition[b]	No. of particles observed in γ chambers 0	1	2 (type A)	2 (type B)	3 (type C)	A+C
G	0.0	0.02	0.10	0.12	0.76	0.86
$G+C$	0.0	0.09	0.20	0.17	0.54	0.74
$G+C+V(E)$	0.01	0.16	0.30	0.17	0.36	0.66
$G+C+V(E/1.5)$	0.02	0.21	0.34	0.16	0.27	0.61
$G+C+V(E/2.0)$	0.04	0.30	0.34	0.13	0.19	0.53

[a] These efficiencies are for events in which the detected spectrometer γ ray had $P_\perp > 165$ MeV/c.
[b] G is the geometrical detection factor. C is the γ-ray-conversion probability factor. V is the visibility factor, which is a function of the γ-ray energy E.

the visibility factor, giving the probability that the charged particle left sparks in two or more successive gaps to satisfy the scanning criterion for a track. These calculations are summarized in Table III. Computation of the last two factors is discussed below.

The conversion factor converts the amount of material, in r.l., transversed by each γ ray in the γ chambers to an equivalent number of conversion lengths. It is a function of the incident γ-ray energy, and includes both the processes of pair production and Compton scattering. The accuracy of the conversion factor has been verified with observed γ rays from the $\gamma\gamma$ and type-C events. The $\gamma\gamma$ decay mode, described in Sec. V, left γ rays with lab energies in excess of 250 MeV, and was used to check the accuracy of the conversion factor in the region of high energy, where it assumes its asymptotic value. The γ rays entered the 3-ft vertical chamber at approximately right angles to the plates, and the total number of available conversion lengths was roughly equal from event to event. Thus the number of unconverted γ rays from a given sample of $\gamma\gamma$ events, as a function of the number of conversion lengths traversed in the γ chamber, can be expected to follow an exponential law. Figure 21(a) indicates that this was indeed true for the sample of $\gamma\gamma$ events observed in this experiment.

The situation for low-energy γ rays, as often encountered in the type-C events, was somewhat different. The lab energy of each type-C γ ray observed in the γ chambers was predicted in the fitting scheme and used to calculate the corresponding conversion factor. Unlike the γ rays from $\gamma\gamma$ events, those from the type-C events did not encounter roughly the same number of conversion lengths in the γ chambers because of the large variations in the conversion factor and angle of incidence on the chamber plates. Hence a plot of the number of unconverted γ rays versus conversion lengths traversed for the type-C γ rays would not be expected to follow an exponential law. However, the plot does agree very well with a similar plot for the Monte Carlo generated type-C γ rays, as shown in Fig. 21(b). Thus, the experimental data are in agreement with the conversion factor used in the efficiency calculations over the full γ-energy range found in this experiment.

The visibility factor V describes the probability of seeing two or more contiguous sparks in the track of a converted γ ray. This factor has been computed as a function of the initial γ-ray energy, its angle of incidence with the spark-chamber plates, and the material of the

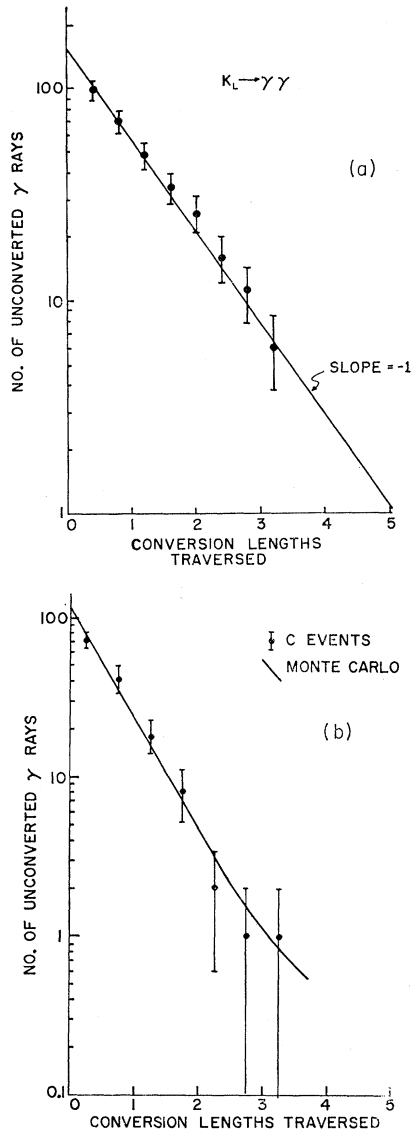

FIG. 21. Plots of number of unconverted γ rays versus number of conversion lengths of material traversed in the γ chambers for (a) a sample of γ rays from $K_L \to \gamma\gamma$ decays, and (b) a sample of γ rays from type-C events.

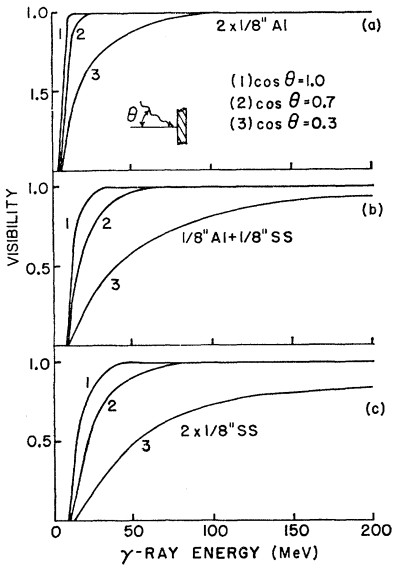

FIG. 22. Visibility function versus γ-ray energy and its angle of incidence θ with the normal of a γ-chamber plate for (a) two $\frac{1}{8}$-in. aluminum plates, (b) one $\frac{1}{8}$-in. aluminum plate and one $\frac{1}{8}$-in. stainless-steel plate, and (c) two $\frac{1}{8}$-in. stainless-steel plates. The curves 1, 2, and 3 in each plot correspond to $\cos\theta = 1.0$, 0.7, and 0.3, respectively. The curves are for the process of pair production. Those for Compton electrons are quite similar.

first two plates encountered by the electron pair. The Monte Carlo calculation for the visibility factor was straightforward and made use of well-established formulas for bremsstrahlung, multiple scattering, and ionization energy loss. No attempt was made to follow the path of an electron beyond the second plate after conversion, and a γ ray was considered visible if at least one of its electrons emerged from the second plate with more than 1-MeV kinetic energy. Details

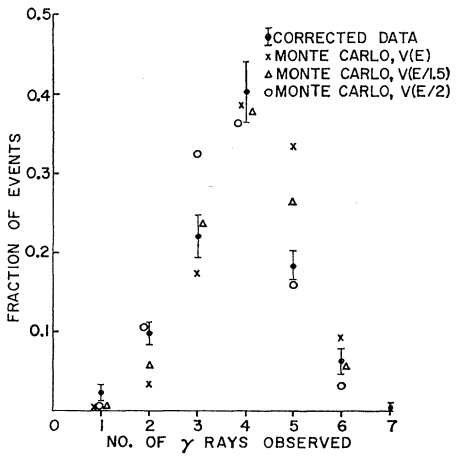

FIG. 23. Distribution in number of γ rays observed for the events in the $K_L \to 3\pi^0$ region, $P_\perp < 165$ MeV/c. Subtractions for the presence of accidental tracks have been made. The Monte Carlo points are calculated with three visibility functions $V(E)$, $V(E/1.5)$, and $V(E/2.0)$.

on this calculation have been given elsewhere.[8] The visibility factor for the different possible combinations of plate material is shown in Fig. 22 as a function of both γ-ray energy and incident angle.

Since the conversion factor used in the efficiency calculations has been shown to be quite accurate, the distribution of the number of γ rays observed in the γ chambers from $K_L \to 3\pi^0$ decay was used as a check on the visibility factor. This check was crude because an evaluation of the scanning efficiency for the $3\pi^0$ events was not made. The fraction of $3\pi^0$ events in which one to six γ rays were observed, with one of these always being seen in the spectrometer, is shown in Fig. 23. Three expected distributions are also presented, corresponding to visibility factors $V(E)$, $V(E/1.5)$, and $V(E/2.0)$, respectively. It should be noted that the visibility for any given γ ray is reduced by substituting a reduced energy in place of its true energy parameter E in the visibility factor V. The agreement between the two distributions seems to be best for a visibility factor with a reduced energy somewhere between $E/1.5$ and $E/2.0$, whereas a visibility factor $V(E)$ was used throughout the efficiency calculations. It is now shown that this is not a serious discrepancy.

It must first be pointed out that the critical region of the visibility curves is that for low-energy γ rays, $E < 50$ MeV. At higher energies, $V(E)$ begins to assume its asymptotic value. Since the γ rays from $2\pi^0$ decay are generally more energetic than those from $3\pi^0$ decay, the detection efficiency for $2\pi^0$ decays is less sensitive to the visibility factor. The experimentally observed ratio of the number of A events to C events can be used as a check on the accuracy of the visibility factor, since this A/C ratio is quite sensitive to the energy dependence of the visibility factor. Experimentally, 39 type-C events and 26 type-A events were observed. However, a correction must be made for the effects of the presence of accidental tracks in the γ chambers. It was found that 20% of all true A events would fit as type-C events with the added presence of an accidental track. This fact reflects the ease with which an accidental track could combine with the spectrometer γ ray to form an apparent spectrometer π^0. The accidental survey indicated that 26% of all events had one accidental track, while an additional 20% has two or more accidental tracks. The corrected experimental A/C ratio is thus 0.8 ± 0.2. The expected A/C ratios for $V(E)$, $V(E/1.5)$, and $V(E/2.0)$, as indicated in Table IV, are 1.0, 1.4, and 1.9, respectively, where the effects of the analysis program have been included. Hence the observed A/C ratio favors the visibility factor $V(E)$. In addition, although the A/C ratio varies quite rapidly as a function of the energy argument in V, the detection efficiency for A+C events remains fairly stable.

The over-all detection efficiency for A+C events, given a spectrometer γ ray with $P_\perp > 165$ MeV/c, has

TABLE IV. Efficiency of analysis program.

Type A	γ ray converting in first aluminum plate	0.07	
	$\lvert p_4-\tilde{p}_4\rvert>8$ MeV	0.19	0.30
	Best-fit decay vertex outside fiducial volume	0.04	
	Fraction of type B analyzed as type A = 0.39		
	Fraction of type C analyzed as type A = 0.11		
Type C	More than one γ ray converting in first or second aluminum plate	0.02	
	Fraction of events with a best fit $\chi^2 \geq 9$	0.09	0.14
	Fraction of events with $\chi^2<9$, but $m^*<350$ MeV, or $m^*>650$ MeV	0.03	

Visibility factor	Calculated efficiency before analysis Type A	Type C	Calculated efficiency including analysis Type A	Type C	ϵ_{AC}	A/C
$V(E)$	0.30	0.36	0.32	0.31	0.63	1.0
$V(E/1.5)$	0.34	0.27	0.33	0.23	0.56	1.4
$V(E/2.0)$	0.34	0.19	0.31	0.16	0.47	1.9
$V=1.0$	0.20	0.54	0.27	0.46	0.73	0.6

been calculated to be

$$\epsilon_{AC}=0.63\pm0.10. \quad (18)$$

The value $\epsilon_{AC}=0.63$ differs from 0.66, the raw efficiency as given in Table III, because of small inefficiencies and shifting of categories in the kinematic fitting procedures. These effects are summarized in Table IV, and were established by analyzing the Monte Carlo generated events with the same analysis program used for the experimental events. The error assigned to ϵ_{AC} is probably an overestimate, since the range of ϵ_{AC} corresponding to a visibility factor in the range $V=V(E/2.0)$ to $V=1.0$ is 0.47–0.73, as summarized in Table IV. However, since ϵ_{AC} plays a vital role in the final determination of $|\eta_{00}|$, it is felt that a safe error is necessary.

The total number of spectrometer triggers arising from $K_L \to \pi^0\pi^0$ decays, $N_{2\pi^0}$, can now be computed. From Eq. (15), the total number of A+C events with $P_\perp>165$ MeV/c is $N_{AC}=57\pm9$. The spectrometer efficiency calculations indicate that 0.57 ± 0.02 of all $2\pi^0$ triggers have $P_\perp>165$ MeV/c. Thus, with Eq. (18), we find

$$N_{2\pi^0}=(N_{AC}/\epsilon_{AC})[1/(0.57\pm0.02)] =161\pm37. \quad (19)$$

D. 3π Events

The $K_L \to 3\pi^0$ and $K_L \to \pi^+\pi^-\pi^0$ events observed in the spectrometer are used as normalization for $K_L \to 2\pi^0$, as well as for the other decay modes described in Secs. V–VII. The number of 3π events observed in the spectrometer was taken as the number of events under the peak in the 3π region, $P_\perp<165$ MeV/c, after subtractions for $\gamma\gamma$, $2\pi^0$, and interaction-background events. Background from other γ-ray-yielding decay modes of the K_L was negligible. The $\gamma\gamma$ and $2\pi^0$ subtractions were made using the shape of the $P_\perp$ spectra predicted by Monte Carlo calculations, normalized to the number of such observed events with $P_\perp>165$ MeV/c. The interaction-background subtraction, which was the major subtraction, was based on the $P_\perp$ spectrum observed in the Hevimet run. The Hevimet attenuated the beam by 12%, and virtually all of the observed events originated in this piece of metal. The $P_\perp$ spectral shape obtained from the Hevimet data was corrected for free-decay events and normalized to the number of background events with $P_\perp>165$ MeV/c. The corresponding spectrum with $P_\perp<165$ MeV/c was then used as a subtraction for interaction background, since the detection efficiency of the spectrometer as a function of $P_\perp$ was rather insensitive to the Z coordinate of the decay point.

The over-all subtraction is only ~8% of all the events observed in the 3π region. Figure 24(a) shows the $P_\perp$ distribution for the helium data before the subtraction, and Fig. 24(b) shows the same after the subtraction for $2\pi^0$, $\gamma\gamma$, and interaction background. The agreement with the Monte Carlo distribution is excellent, with a χ^2 of 7.3 for eight degrees of freedom ($P_\perp<170$ MeV/c). A further check that the sample of 3π events is pure is provided by the observed branching ratio (see Appendix A)

$$\Gamma(K_L \to \pi^+\pi^-\pi^0)/\Gamma(K_L \to \pi^0\pi^0\pi^0)=0.58\pm0.10, \quad (20)$$

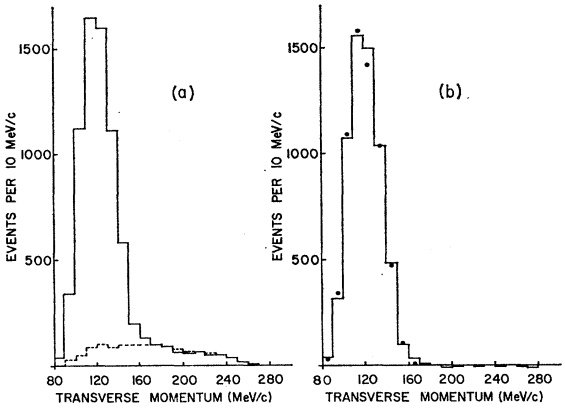

FIG. 24. (a) Transverse momentum spectrum for γ rays observed in the spectrometer during the full-field helium run. The dashed curve denotes the contribution from $2\pi^0$, $\gamma\gamma$, and interaction background events. (b) Transverse momentum spectrum after subtraction for $2\pi^0$, $\gamma\gamma$, and interaction background events. The dots denote the Monte Carlo prediction, normalized to the observed number of events.

which is in good agreement with the best current value of 0.60 ± 0.03.[9]

The number of 3π events, which is the sum of $3\pi^0$ and $\pi^+\pi^-\pi^0$ events, observed in the spectrometer is

$$N_{3\pi}=6077\pm85. \tag{21}$$

E. Calculation of Branching Ratio $\Gamma(K_L\to 2\pi^0)/\Gamma(K_L\to \text{all})$

The spectrometer-efficiency calculations, summarized in Table II, give the efficiency of the spectrometer for the detection of a single γ ray from $K_L\to 2\pi^0$ decay as[10]

$$\epsilon_{2\pi^0}=(9.73\pm0.49)\times10^{-3}. \tag{22}$$

The corresponding efficiencies for the 3π decay modes are

$$\epsilon_{3\pi^0}=(1.02\pm0.05)\times10^{-3} \tag{23}$$

and

$$\epsilon_{\pi^+\pi^-\pi^0}=(0.57\pm0.03)\times10^{-3}. \tag{24}$$

Using a branching ratio[9]

$$\begin{aligned}R'&=\Gamma(K_L\to\pi^+\pi^-\pi^0)/\Gamma(K_L\to 3\pi^0)\\&=0.60\pm0.03,\end{aligned} \tag{25}$$

the efficiency for detecting a single γ ray from 3π decays is

$$\begin{aligned}\epsilon_{3\pi}&=(6\epsilon_{3\pi^0}+2R'\epsilon_{\pi^+\pi^-\pi^0})/(6+2R')\\&=(0.946\pm0.047)\times10^{-3},\end{aligned} \tag{26}$$

where the factors of 6 and 2 refer to the number of γ rays available in the $3\pi^0$ and $\pi^+\pi^-\pi^0$ decays, respectively. The expected number of γ rays from the 3π decay modes is $(6+2R')\times\Gamma(K_L\to 3\pi^0)/\Gamma(K_L\to \text{all})$, while the expected number of γ rays from the $2\pi^0$ decay mode is $4\Gamma(K_L\to 2\pi^0)/\Gamma(K_L\to \text{all})$. Hence, from Eq. (19) and (21)–(26), we have

$$\begin{aligned}\frac{\Gamma(K_L\to 2\pi^0)}{\Gamma(K_L\to 3\pi^0)}&=\frac{N_{2\pi^0}}{N_{3\pi}}\frac{[\frac{1}{4}(6+2R')]}{\epsilon_{2\pi^0}}\\&=(4.6\pm1.1)\times10^{-3}.\end{aligned} \tag{27}$$

With Eq. (27) and the branching ratio[9]

$$\Gamma(K_L\to 3\pi^0)/\Gamma(K_L\to \text{all})=0.209\pm0.011, \tag{28}$$

the branching ratio for $2\pi^0$ is found to be

$$\Gamma(K_L\to 2\pi^0)/\Gamma(K_L\to \text{all})=(0.97\pm0.23)\times10^{-3}. \tag{29}$$

From Eq. (2), we have

$$\begin{aligned}|\eta_{00}|^2&=\Gamma(K_L\to 2\pi^0)/\Gamma(K_S\to 2\pi^0)\\&=\frac{\Gamma(K_L\to 2\pi^0)}{\Gamma(K_L\to \text{all})}\frac{\Gamma(K_L\to \text{all})}{\Gamma(K_S\to \text{all})}\\&\quad\times\left(\frac{\Gamma(K_S\to 2\pi^0)}{\Gamma(K_S\to \text{all})}\right)^{-1}.\end{aligned} \tag{30}$$

With Eq. (29) and the values[11]

$$\begin{aligned}&\Gamma(K_S\to 2\pi^0)/\Gamma(K_S\to \text{all})=0.316+0.011,\\&\tau_S=\Gamma(K_S\to \text{all})^{-1}=(0.862\pm0.006)\times10^{-10}\text{ sec},\\&\tau_L=\Gamma(K_L\to \text{all})^{-1}=(5.38\pm0.20)\times10^{-8}\text{ sec},\end{aligned} \tag{31}$$

the quantity

$$|\eta_{00}|^2=(4.9\pm1.2)\times10^{-6} \tag{32}$$

follows from Eq. (30). This corresponds to

$$|\eta_{00}|=(2.2\pm0.3)\times10^{-3}. \tag{33}$$

V. $K_L\to\gamma\gamma$ DECAY

Candidates for this decay mode originated in the sample of 629 spectrometer events with transverse momentum above 165 MeV/c. This is the same set of events analyzed for $K_L\to\pi^0\gamma\gamma$ and $K_L\to\pi^0\pi^0$ decays. Although final candidates for the $\pi^0\gamma\gamma$ and $\pi^0\pi^0$ decay modes were taken from the 381 events with $E_{\text{c.m.}}$ below 240 MeV, this selection was done after measurement of the γ-chamber film. Thus, data for $K_L\to\gamma\gamma$ were measured concurrently with data for these other modes.

Measurement of the 629 selected events has been described above. Those events which later proved to be $\gamma\gamma$ decays had, typically, a track traversing 5–10 gaps in the γ chamber opposite the spectrometer. This was expected since the γ-ray lab energies were generally above 250 MeV. Care was taken, however, to measure events with even a single two-spark track, since the source of background spectrometer triggers was of considerable interest. For this reason, we believe there were no $\gamma\gamma$ events lost because they did not show an obvious high-energy converted γ ray.

As was done for the other decay modes, the K_L decay point was determined in the fitting process. The decay point was assumed to lie along the line of flight of the spectrometer γ ray in the region where it crossed the beam volume. Trial decay points were selected at 0.5-in. intervals along this line segment and a fit was tried at each point. The direction of a γ ray in the steel γ chambers was taken as the line from the trial decay point to the first measured point on the track. The two photon directions were then transformed to the c.m. system of the decaying particle by using the measured TOF. The angle between the two photons in this system was computed, and the decay point which resulted in the photons being most nearly collinear was selected. The fit to $K_L\to\gamma\gamma$ was tried for all measured tracks regardless of other decay hypotheses which might be satisfied. The inclusion of possible backgrounds is

[9] I. A. Budagov, H. Burmeister, D. C. Cundy, W. Krenz, G. Myatt, F. A. Nezrick, H. Sletten, G. H. Trilling, W. Venus, H. Yoshika, B. Aubert, P. Heusse, I. LeDong, E. Nagy, C. Pascaud, L. Behr, P. Beillière, G. Boutang, and J. van der Velde, Nuovo Cimento **57A**, 182 (1968).

[10] Note that these efficiencies should be considered only in a relative sense. No effort was made to set the absolute scale in the detailed Monte Carlo calculations.

[11] N. Barash-Schmidt, A. Barbaro-Galtieri, L. R. Price, A. H. Rosenfeld, P. Söding C. G. Wohl, M. Roos, and G. Conforto, Rev. Mod. Phys. **41**, 109 (1969).

discussed below. After fitting, events were rejected which had the γ ray converting in either of the first two aluminum plates.

In this fitting scheme the momentum measurement of the spectrometer was not used. Figure 25 shows the distribution in $E_{\text{c.m.}}$ and its correlation with $\cos\theta_{\gamma\gamma}$, the measure of collinearity in the c.m. system. The smooth curve in the distribution projected on the $E_{\text{c.m.}}$ axis is the Monte Carlo prediction for $K_L \to \gamma\gamma$. The Monte Carlo curve is broadened to a standard deviation of 3.5% from the predicted 2.4%. This discrepancy results from a slight misalignment of the two cells of the wide-gap spark chamber in the reconstruction program. If one assumes that the collinearity distribution has an exponential shape in $\cos\theta_{\gamma\gamma}$, the observed standard deviation is 30 mrad compared to the predicted 25 mrad.

The kinematic region used to obtain the final $K_L \to \gamma\gamma$ candidates was $215 < E_{\text{c.m.}} < 270$ MeV, $P_\perp > 165$ MeV/c, and $-1.00 \leq \cos\theta_{\gamma\gamma} < -0.99$. There were 116 events observed in this region. The observed TOF distribution for events with $\cos\theta_{\gamma\gamma} < -0.99$ and the distribution of decay points both served as useful calibrations for the search for the decay $K_S \to \gamma\gamma$, as described in Sec. VI.

Consider now the contribution from background sources. If one assumes a flat background, normalized to the number of events in excess of Monte Carlo predictions below 215 MeV, then the contribution in the $E_{\text{c.m.}}$ region defined above is less than 10%. In addition, the background must have a cutoff below 260 MeV because no events were seen above this energy.

The contribution from beam interactions in the helium gas can be estimated from SF_6 data where the interaction rate was expected to be 14 times[7] higher. The SF_6 data gave 16 ± 4 events fitting $K_L \to \gamma\gamma$ according to the above criteria. This yield corresponds to 122 ± 28 events for an SF_6 run of the same duration as the free decay. Thus there is no evidence of beam-interaction background.

A Monte Carlo simulation with the observed energy resolution rules out any contribution from $K_L \to 3\pi$ decays where the K_L is traveling in the beam direction. The background analysis given previously for $K_L \to \pi^0\pi^0$ finds no evidence for an off-axis component of the beam.

The most probable background comes from $K_L \to \pi^0\pi^0$ decays. A study of events which give fits to both the decay hypotheses $K_L \to \pi^0\pi^0$ and $K_L \to \gamma\gamma$ indicates that there are only two such events in the kinematic region defined above. Both events are the weak type-B fits to $K_L \to \pi^0\pi^0$. They are included in the $\gamma\gamma$ sample. A Monte Carlo study normalized to the observed number of $\pi^0\pi^0$ decays indicates that we can expect one $\pi^0\pi^0$ event to fit in the kinematic region defined above. This study gives the dashed curve in Fig. 25 which is the expected event level when $K_L \to \pi^0\pi^0$ background is included. Accordingly, the final number of $\gamma\gamma$ candidates is taken as 115 ± 11.

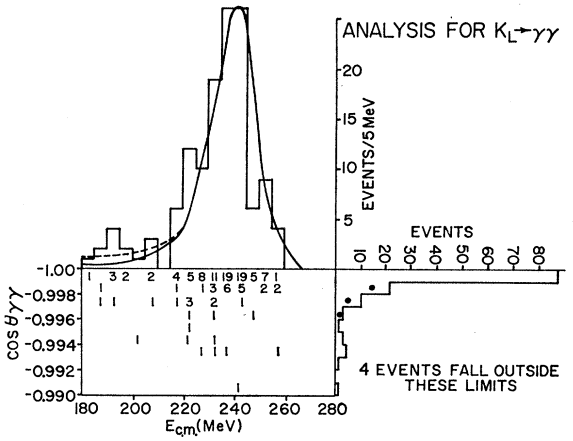

FIG. 25. Plot for $K_L \to \gamma\gamma$ candidates of the cosine of the angle between the γ-ray directions in the K_L c.m. system at the best-fit decay point, versus the c.m. energy of the spectrometer γ ray. The projections of the data on the two axes are shown together with Monte Carlo predictions. The solid line and closed circles indicate Monte Carlo precictions for $K_L \to \gamma\gamma$. The dashed curve is explained in the text.

A Monte Carlo study of the response of the apparatus to $K_L \to \gamma\gamma$ decays indicates that 0.828 ± 0.032 of the $\gamma\gamma$ decays, detected in the kinematic region defined above, show a converted γ ray in the steel-plate chambers and satisfy the fitting criteria. The 17% inefficiency results from 10% of the events which have no conversion in the chambers, and 7% which convert in one of the first two plates. Fewer than 1% of all events fail to fit. The fraction of all $K_L \to \gamma\gamma$ events detected in the spectrometer with $215 < E_{\text{c.m.}} < 270$ and $P_\perp > 165$ MeV/c is calculated to be 0.884 ± 0.019. Thus the total number of $K_L \to \gamma\gamma$ events observed in the spectrometer is $N_{\gamma\gamma} = 157\pm16$.

The efficiency of the spectrometer obtained from Monte Carlo calculations for the $\gamma\gamma$ decay mode, $\epsilon_{\gamma\gamma}$, is given in Table II. Using Eq. (26), one finds $\epsilon_{3\pi}/\epsilon_{\gamma\gamma} = 0.0241\pm0.0017$. Normalization is obtained from the total number of 3π decays observed, $N_{3\pi} = 6077\pm85$, as given in Eq. (21). Finally, with Eq. (25), we have

$$\frac{\Gamma(K_L \to \gamma\gamma)}{\Gamma(K_L \to \pi^0\pi^0\pi^0)} = \frac{N_{\gamma\gamma}}{N_{3\pi}} \left[\tfrac{1}{2}(6+2R')\right] \frac{\epsilon_{3\pi}}{\epsilon_{\gamma\gamma}} = (2.24\pm0.28)\times10^{-3}. \quad (34)$$

Using $\Gamma(K_L \to 3\pi^0)/\Gamma(K_L \to \text{all modes}) = 0.209\pm0.011$,[9] we find

$$\frac{\Gamma(K_L \to \gamma\gamma)}{\Gamma(K_L \to \text{all modes})} = (4.7\pm0.6)\times10^{-4}. \quad (35)$$

VI. $K_S \to \gamma\gamma$ DECAY

Thirteen rolls of film (~40 000 pictures) were taken with the helium bag removed from the decay volume and a $14.5\times10.06\times0.566$-in. Hevimet (~ tungsten) slab inserted in the beam, 9 in. upstream from the center of the apparatus. The data were

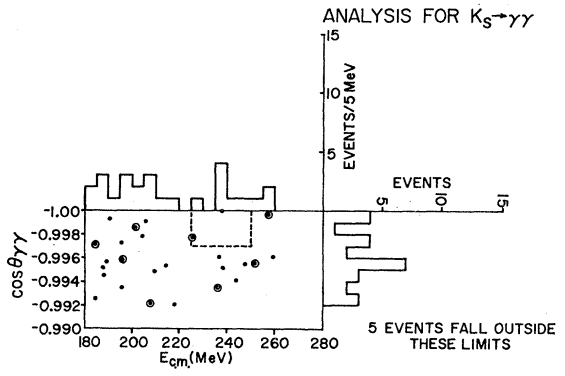

FIG. 26. Plot for $K_S \to \gamma\gamma$ candidates of the cosine of the angle between the two γ-ray directions in the K_L c.m. system at the best-fit decay point versus the c.m. energy of the spectrometer γ ray. A circled dot indicates an event with TOF <10 nsec. The dashed rectangle encloses the region from which the final candidates were selected.

analyzed for $K \to \gamma\gamma$ decays from the regenerator region. To compute the branching ratio, the relative intensity of the regenerated K_S beam was estimated by optical-model calculations. Normalization was obtained from the number of 3π decays observed upstream from the regenerator.

The spectrometer data were analyzed in the usual fashion, and after the cuts discussed in Sec. III, 4030 events remained. For the 1720 events with $E_{c.m.}>180$ MeV, the γ-chamber data were scanned. Events were measured if they showed a converted γ ray traversing at least four gaps in the γ chamber opposite the spectrometer. From the free-decay $\gamma\gamma$ analysis where such a criterion was not imposed, it is known that $(96_{-9}^{+4})\%$ of the observed $K_L \to \gamma\gamma$ events satisfied this requirement. There were 404 events left for further analysis. They were measured and fitted to the hypothesis $K \to \gamma\gamma$ in exactly the same way as discussed in Sec. V on $K_L \to \gamma\gamma$. The additional requirement was made, however, that both γ rays involved in a fit must be in

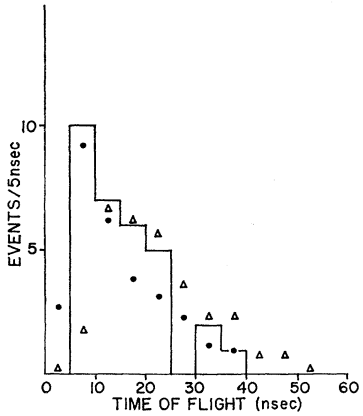

FIG. 27. TOF distribution for $K_S \to \gamma\gamma$ candidates. $\triangle$, TOF distribution for free-decay $K_L \to \gamma\gamma$ data. $\bullet$, TOF distribution for all events originating from the regenerator region of the beam (see text for precise definition).

the laboratory forward hemisphere with respect to the decay point and the beam direction. Since the K_S decay length was typically 1 cm, backward-going γ rays from K_S decays passed through the 4-r.l. regenerator, converted there, and were lost. Only 1.6% of the data was eliminated by this cut, whereas the Monte Carlo study indicated that 24% of the $K \to \gamma\gamma$ events would have at least one γ ray in the backward direction if conversion in the regenerator were neglected.

As candidates for the decay $K_S \to \gamma\gamma$ we consider only events with a fitted decay point in the region $-11<Z<-6$ in. The regenerator was located at $Z=-9.0\pm0.25$ in. The interval was chosen on the basis of the spatial resolution and K_S decay length.

With these requirements we obtain the $E_{c.m.}$-versus-$\cos\theta_{\gamma\gamma}$ plot of Fig. 26. It is to be compared with the corresponding distribution for the free-decay $K_L \to \gamma\gamma$ data shown in Fig. 25.

The TOF spectrum for the 31 events with $\cos\theta_{\gamma\gamma}<-0.99$ is compared in Fig. 27 with the spectrum observed from the free-decay $K_L \to \gamma\gamma$ data, and with the spectrum for all spectrometer events associated with the regenerator. The $K_S \to \gamma\gamma$ candidates show a strong excess compared to the free-decay events for TOF's less than 10 nsec, corresponding to incident K_L momentum greater than 450 MeV/c. This excess is typical of spectrometer triggers from beam interactions in the regenerator. Regeneration of K_S is expected to produce no such enhancement.[12] Because of the excess at short TOF, we only consider events with TOF >10 nsec. The events eliminated are shown circled in Fig. 26.

Final candidates for the decay $K_S \to \gamma\gamma$ are taken as events which fall in kinematic region $225<E_{c.m.}<255$ MeV, $\cos\theta_{\gamma\gamma}<-0.997$, and TOF >10 nsec. This is the region of highest event density for the free-decay $K_L \to \gamma\gamma$ data of Fig. 25. There remains one candidate.

The data is normalized by the 3π decays observed to come from the beam volume upstream from the regenerator. Events are classified according to whether they come from the upstream region, regenerator region, or downstream region. The separation is made on the basis of the Z coordinates of the points at which the spectrometer γ ray trajectory crosses the two sides of the beam volume. If both crossings occur for $Z<-12$ in., an event is assigned to the upstream region. If both crossings occur for $Z>0$ in., the event is classified as a downstream decay. The remaining events are assigned to the regenerator region.

The transverse-momentum spectra obtained for events from the three regions are shown in Fig. 28. The data obtained outside the regenerator region are compared with the corresponding data from a free-decay run in which the helium bag was removed and the beam passed through air in the decay volume. The spectra of Figs. 28(a) and 28(b) are good fits to the expected

[12] See the dependence of regenerated intensity on K_L momentum, given in Table VIII.

shapes and show no evidence of contamination from beam interactions in the regenerator.

These results can be used to measure the beam attenuation by the regenerator. The observed attenuation provides a rough check on the optical-model calculation used to predict the features of the regeneration process. There are 702 and 274 observed events from the upstream and downstream regions, respectively, with a transverse momentum below 165 MeV/c. For this number of upstream decays, the free-decay data taken with air predicts 313±22 downstream events. The attenuation is thus (12±8)%. The calculation discussed in Appendix B predicts 13%.

To use the upstream 3π decays for normalization, background events must be eliminated. This is done by considering only events having $P_\perp < 160$ MeV/c and TOF > 25 nsec. These cuts have been found effective in eliminating background. We observe 253 upstream decays with $P_\perp < 160$ MeV/c and TOF > 25 nsec. A corresponding cut on the free-decay data leaves 1211 (20%) of the 6077 observed 3π events. We conclude that the duration of the regenerator run was equivalent to that of a free-decay run with 1270±80 observed 3π events. This number, together with the $K_L \to 3\pi$ efficiency for free-decay data, is used for normalization.

The same system of computer programs was used to determine the detection and fitting efficiencies for the decay $K_S \to \gamma\gamma$ as was used for $K_L \to \gamma\gamma$. The only differences were that the decay point was fixed at $Z = -9$ in. and events were rejected if either γ ray appeared in the backward hemisphere. Efficiencies were computed with the K_S directed along the beam direction, as is the case for coherent regeneration, and also with the K_S distributed over a narrow angular interval about the beam direction as one expects for the incoherently regenerated K_S. The size of this interval was a function of the K_L momentum for each event (see Appendix B), and is typically 9° for 250-MeV/c K_L.

Sources of background to be considered are $K_L \to \gamma\gamma$ events in the region selected for $K_S \to \gamma\gamma$ candidates, decays $K_S \to \pi^0\pi^0$, and inelastic beam interactions in the regenerator.

The data for $K_L \to \gamma\gamma$ shows eight events in the beam volume chosen for $K_S \to \gamma\gamma$ decays. Accounting for the relative duration of the two runs and the effect of the regenerator, we expect to observe 1.1±0.06 $K_L \to \gamma\gamma$ events.

Using the efficiencies given in Table V and performing a calculation similar to that shown below for the final branching ratio, we estimate the number of background events from incoherently produced K_S decaying to $\pi^0\pi^0$ to be 0.8±0.5.

The contribution from beam interactions in the regenerator is difficult to evaluate. Their most striking feature, however, is a TOF spectrum strongly peaked at short times. After the elimination of events with TOF < 10 nsec, the remaining 25 events of Fig. 27 show a TOF spectrum similar to the free-decay data. Because of this correspondence and the fact that the background estimates above account for the one final candidate observed, no further consideration is given to this background source.

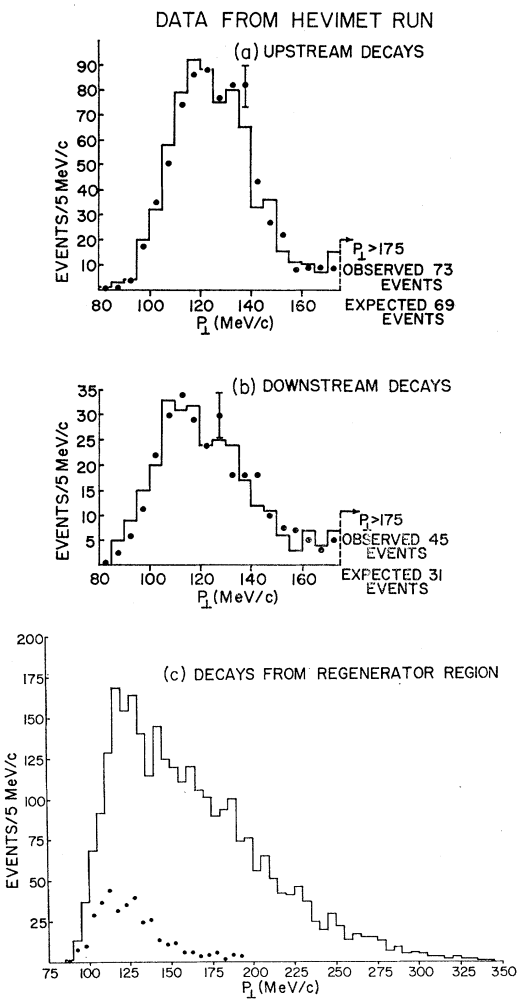

FIG. 28. (a) Transverse momentum distribution for events originating in the beam volume upstream from the regenerator (see text for precise definition). ● indicates the expected distribution with no regenerator. These latter data were obtained from a run with the beam passing through air in front of the apparatus. Normalization is to the same total number of events in this region. (b) Transverse momentum distribution for events originating downstream from the regenerator. ●, same as in (a). (c) Transverse momentum distribution for events originating from the regenerator region. ●, expected from this region with no regenerator. These data are from the run with the beam passing through air. Normalization is to the same number of events from the upstream region.

The over-all number of predicted background events is taken to be two. The expected background of two events and the single event observed give two events as the 90% confidence limit on the number of true $K_S \to \gamma\gamma$ events. We combine this number with the computed efficienceis to obtain an upper limit on the branching ratio.

TABLE V. Efficiencies for $K_S \to \gamma\gamma$ study.

Mode	Raw efficiency[a]	Angular efficiency correction	Efficiency for γ in forward hemisphere	Over-all spectrometer efficiency	γ-chamber efficiency[b]
$K \to \gamma\gamma$ (coherent K)[c]	0.0948	0.879	0.764	0.0636	0.55
$K \to \gamma\gamma$ (incoherent K)[d]	0.0930	0.872	0.772	0.0626	0.13
$K \to \pi^0\pi^0$ (coherent K)	0.0256	0.914	0.796	0.0186	<0.003
$K \to \pi^0\pi^0$ (incoherent K)	0.0190	0.894	0.812	0.0138	0.006

[a] This is the relative spectrometer efficiency for detecting a single γ ray. The coordinate of the decay point was located at $Z=-9$ in. A requirement of TOF >10 nsec is imposed.
[b] The requirements are that (i) γ ray detected in γ chambers is in forward hemisphere, (ii) observed γ-ray track shows four or more contiguous sparks (factor obtained from $K_L \to \gamma\gamma$ data), (iii) $-1.0 \leq \cos\theta_{\gamma\gamma} < -0.997$, and (iv) $225 < E_{\text{c.m.}} < 255$ MeV.
[c] The K was along the beam direction.
[d] The K direction was distributed over a narrow angular range typical of incoherent regeneration (see Appendix B).

In the Monte Carlo simulation of free decay, the relative efficiencies were computed on the basis that a decay occurred in the 110-in. interval $-65<Z<45$ in. For the computed efficiencies to detect regenerated decays, the decay was required to occur 56 in. from the start of the decay region, i.e., at $Z=-9$ in. This is valid because the mean K_S decay length is 0.56 in. Thus, assuming no interference between $K_S \to \gamma\gamma$ and $K_L \to \gamma\gamma$, we have

$$N_{3\pi} \propto N_{K_L}(1-e^{-110/\Lambda_L})\frac{\Gamma(K_L \to 3\pi^0)}{\Gamma(K_L \to \text{all})}(6+2R')\epsilon_{3\pi}, \quad (36)$$

$$N_{\gamma\gamma} \propto N_{K_L}e^{-56/\Lambda_L}(I_{\text{coh}}\eta_{\text{coh}}+I_{\text{inc}}\eta_{\text{inc}}) \times\frac{\Gamma(K_S \to \gamma\gamma)}{\Gamma(K_S \to \text{all})}(2\epsilon_{\gamma\gamma})\epsilon_s\epsilon_r \quad (37)$$

$$\frac{\Gamma(K_S \to \gamma\gamma)}{\Gamma(K_S \to \text{all})}=\frac{N_{\gamma\gamma}}{N_{2\pi}}\frac{1-e^{-110/\Lambda_L}}{e^{-56/\Lambda_L}(I_{\text{coh}}\eta_{\text{coh}}+I_{\text{inc}}\eta_{\text{inc}})} \times[\tfrac{1}{2}(6+2R')]\frac{\epsilon_{3\pi}}{\epsilon_{\gamma\gamma}\epsilon_s\epsilon_r}R, \quad (38)$$

with the following values:

N_{K_L} is the number of K_L entering the region $-65<Z<45$ in.

Λ_L is the mean decay length of the K_L (344 in.).

I_{coh} is the intensity of coherent K_S regeneration per incident K_L and is given in Appendix B.

I_{inc} is the intensity of incoherent K_S regeneration per incident K_L and is given in Appendix B.

η_{coh} is the efficiency to detect in the γ chambers and to fit a decay $K_S \to \gamma\gamma$, where the K_S has been regenerated coherently and the spectrometer γ was detected. From Table V, one finds 0.55 ± 0.08.

η_{inc} is the same as η_{coh} except that the K_S was regenerated incoherently. Table V indicates 0.13 ± 0.02.

ϵ_s is the scanning efficiency of 0.91 ± 0.07, as determined by two scans.

$\epsilon_{3\pi}$ is the per-γ-ray spectrometer detection efficiency for $K_L \to 3\pi$, averaged over the relative probability and efficiencies for the decays $K_L \to \pi^0\pi^0\pi^0$ and $K_L \to \pi^+\pi^-\pi^0$, as given in Eq. (26).

$\epsilon_{\gamma\gamma}$ is the per-γ-ray spectrometer detection efficiency for $K \to \gamma\gamma$ at $Z=-9$ in., averaged by the relative probability and efficiency for coherently and incoherently regenerated K_S. From Table V, one obtains 0.0629.

R' is the branching ratio

$$\Gamma(K_L \to \pi^+\pi^-\pi^0)/\Gamma(K_L \to \pi^0\pi^0\pi^0)=0.60\pm0.03.^9$$

$N_{3\pi}$ is the effective number of 3π decays observed $=1270\pm80$.

$N_{\gamma\gamma}$ is the number of events for $K_S \to \gamma\gamma < 2$ (90% confidence).

ϵ_r is the fraction of the beam cross section covered by the regenerator $=0.87$.

R is the branching ratio $\Gamma(K_L \to 3\pi^0)/\Gamma(K_L \to \text{all})$ $=0.209\pm0.011$.[9]

Using these data in the above expression for the branching ratio, we find

$$\Gamma(K_S \to \gamma\gamma)/\Gamma(K_S \to \text{all}) < 1.2\%, \quad (39)$$

with 90% confidence.

This analysis has assumed that the decays $K_L \to \gamma\gamma$ and $K_S \to \gamma\gamma$ are incoherent. The limit is somewhat insensitive to interference effects since 64% of the detected K_S signal arises from incoherent regeneration and is not subject to interference. If one asumes that the $K_L \to \gamma\gamma$ amplitude and regenerated $K_S \to \gamma\gamma$ amplitude were totally constructive, the limit becomes 0.68%; if they were totally destructive, then the limit is 2.1%. Hence the absolute upper limit set by this experiment is

$$\Gamma(K_S \to \gamma\gamma)/\Gamma(K_S \to \text{all}) < 2.1\%, \quad (40)$$

with 90% confidence.

VII. $K_L \to \pi^0\gamma\gamma$ DECAY

With present techniques, any experimental study of this decay mode is dependent on a knowledge of the matrix element. The exact form of the matrix element is unknown, but part of its functional dependence on the kinematic variables of the decay can be deduced on symmetry principles.

The variables available for its construction are $F_{\mu\nu}$ and $F_{\mu\nu}'$, the field-strength tensors of the two photons, and q_μ, the pion four-momentum. These should be combined to yield a matrix element which is Lorentz-invariant, gauge-invariant, CP-invariant, and sym-

metrical in the two photons. One then writes

$$M = G_1 F_{\mu\nu} F_{\mu\nu}' + G_2 F_{\mu\nu} F_{\mu\sigma}' q_\nu q_\sigma + \text{terms of higher order in } q_\mu. \quad (41)$$

The coefficients G_i are Lorentz scalars. Since the order of a term in the four-momentum q_μ indicates the corresponding pion angular momentum, terms beyond the first will be neglected on the grounds of suppression by an angular momentum barrier. Using the gauge-invariant form $F_{\mu\nu} = k_\mu \epsilon_\nu - k_\nu \epsilon_\mu$, squaring, and summing over polarizations, one obtains

$$|M|^2 = |G_1|^2 m_{\gamma\gamma}^4, \quad (42)$$

where $m_{\gamma\gamma}$ is the effective mass of the γ-ray system. The coefficient G_1 is a model-dependent function of the Lorentz invariants of the problem. For lack of better information, G_1 is taken as constant in this study.

When this matrix element is combined with phase space, the c.m. γ-ray energy spectra of Fig. 29 are obtained. The effective mass distribution of the two direct photons is shown in Fig. 30.

The following results are for an experimental analysis based on the $m_{\gamma\gamma}^4$ matrix element for the decay $K_L \to \pi^0\gamma\gamma$. Candidates for this decay mode were drawn from the same sample of events as those for the decay $K_L \to \pi^0\pi^0$, where the γ-chamber data were measured for the 629 events with a transverse momentum above 165 MeV/c.

Events which were fitted for $K_L \to \pi^0\gamma\gamma$ were required to have three γ rays converted in the γ chambers. This is the same set of events as was subjected to a type-C fit for $K_L \to \pi^0\pi^0$. Track criteria and treatment of accidental tracks have been described in Sec. IV. The two measurements yielded a total of 111 events with $P_\perp > 165$ MeV/c, $E_{\text{c.m.}} < 240$ MeV, three or four measured particles in the γ chambers, and no more than one charged particle observed. These events would have had a two-constraint fit to the decay hypothesis

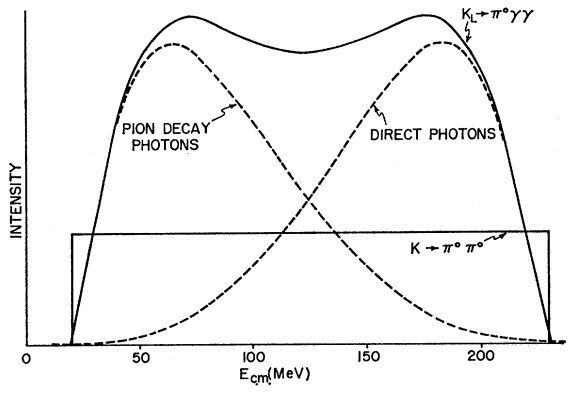

FIG. 29. Center-of-mass energy spectrum for γ rays from $K_L \to \pi^0\gamma\gamma$, based on an $m_{\gamma\gamma}^4$ matrix element. Also shown for comparison is the spectrum from $K_L \to \pi^0\pi^0$. Normalization is arbitrary.

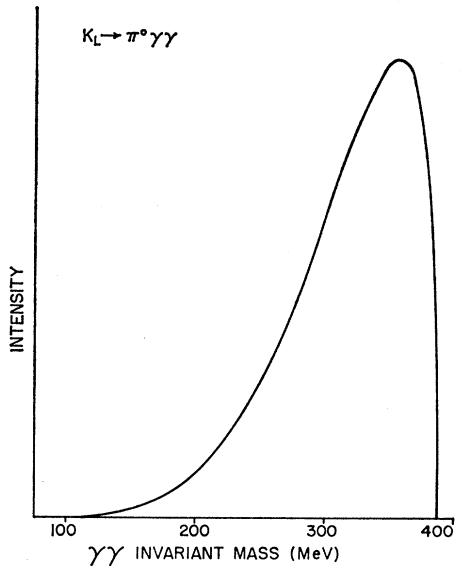

FIG. 30. Distribution of $m_{\gamma\gamma}$ based on $m_{\gamma\gamma}^4$ matrix element.

$K_L \to \pi^0\gamma\gamma$ if the decay point were known, but since this point was determined by fitting, only one kinematic constraint remained. Actually, there is also the geometrical constraint that the decay point must be in the beam region. Kinematic fitting was based on the assumption that the γ ray seen in the spectrometer was one of the direct γ rays and not associated with the decay of the π^0. For γ rays with $E_{\text{c.m.}} > 165$ MeV, this assumption is true 91.8% of the time if one neglects apparatus efficiency and resolution. When the spectrometer efficiency and observed resolution are folded in and the limit is set at $P_\perp > 165$ MeV/c, the assumption is true with a 95.1% frequency. These probabilities depend on the matrix element assumed for the decay, but as discussed above the choice is fairly reasonable.

In fitting an event, all possible combinations of three tracks in the γ chambers were tried. Within a combination, each track was tried in turn as the second direct photon. A χ^2 statistic was computed for each fit and the fit giving the lowest over-all χ^2 was retained.

Because of the poor directional information of the γ-ray tracks, the decay point was obtained by fitting as has been described for the other decay modes. In the notation of Sec. IV, the χ^2 statistic, indicating the goodness of fit of the particular track combination and decay point, was

$$\chi^2 = \frac{(m^* - m_K)^2}{\sigma_K^2} + \frac{(m_{12} - m_\pi)^2}{\sigma_\pi^2},$$

$$\sigma_K = 10 \text{ MeV}, \ \sigma_\pi = 10 \text{ MeV}. \quad (43)$$

Thus, the configuration chosen gives the incident particle mass close to the K mass, and the mass of a pair of γ rays, not including the spectrometer γ ray, close to the π^0 mass. Fitting in this way, we expect to

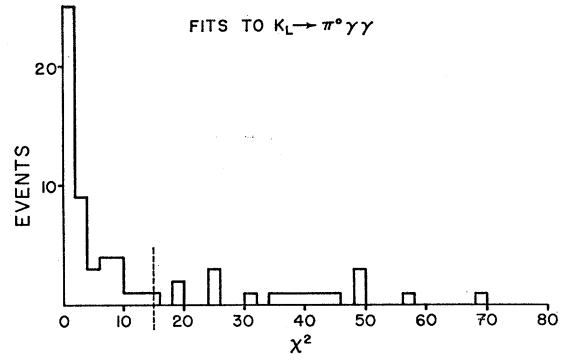

FIG. 31. Distribution of χ^2 minima for fitting events to the hypothesis $K_L \to \pi^0\gamma\gamma$. The dashed line shows where the χ^2 cut was imposed.

detect both $K_L \to \pi^0\pi^0$ and $K_L \to \pi^0\gamma\gamma$. The separation is achieved on the basis of m_{34}, the effective mass of the pair of photons which includes the spectrometer γ ray.

A selection was also made based on the minimum χ^2 for each event. Figure 31 shows the distribution of χ^2 for the 66 events, out of an original 111. These 66 events have a minimum χ^2 at a point no more than 2 in. outside the physical beam volume and fit with a positive track momentum. In setting the weights σ_K and σ_π for the terms of the χ^2 statistic, the relative sizes were determined by Monte Carlo calculations, but the magnitudes do not necessarily represent a standard deviation. The cut on χ^2 is determined from the data. The distribution is flat above a χ^2 of 15, so a cut is imposed at this point. There are 47 events remaining. They are found to include 35 of the 39 final type-C candidates for the decay $K_L \to \pi^0\pi^0$, as described in Sec. IV.

Figure 32 shows the $\gamma\gamma$ effective mass for the pair of photons which was not constrained to have a π^0 mass. A Monte Carlo simulation has been made to study the detection and fitting of both $K_L \to \pi^0\gamma\gamma$ and $K_L \to \pi^0\pi^0$ decays by this scheme. The resulting distributions are also given in Fig. 32. The expected $\pi^0\pi^0$ distribution is normalized to the 39 events with m_{34} <240 MeV. A Monte Carlo study indicates that $(70\pm8)\%$ of the $\pi^0\gamma\gamma$ data should lie above this limit. There are eight observed events with $m_{34}>240$ MeV, while seven are expected from $\pi^0\pi^0$ decay. These $\pi^0\pi^0$ Monte Carlo events have a high mass because the best χ^2 is obtained from a fit with the γ rays mispaired.

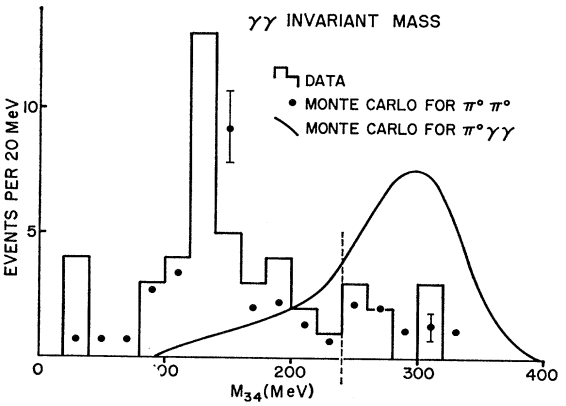

FIG. 32. Distribution of m_{34} for events fit to the hypothesis $K_L \to \pi^0\gamma\gamma$. ● indicates the results when Monte Carlo $K_L \to \pi^0\pi^0$ events are fitted for $K_L \to \pi^0\gamma\gamma$. The sold line indicates the Monte Carlo prediction for $K_L \to \pi^0\gamma\gamma$ events, with $m_{\gamma\gamma}{}^4$ matrix element.

The effect of interactions in the helium-filled beam volume was studied by replacing the helium with SF_6 gas. Among these data, eight events were found using this fitting scheme with $m_{34}<240$ MeV, and three events were found with $m_{34}>240$ MeV. From the helium-free decay data we would expect 1.4 ± 0.7 events above 240 MeV for eight events below this level. From the relative duration of the helium and SF_6 data runs of ~7, and the relative interaction rate in SF_6 compared to helium of ~14,[7] we expect $\sim0.7\pm1$ background events above 240 MeV in the helium data. Other independent background studies were outlined in Sec. II. None of the tests showed any other significant background source. Thus, the eight events observed are fully consistent with the seven events expected from $K_L \to \pi^0\pi^0$ and one event expected from beam interactions in the helium.

A 90% confidence limit on the number of signal events, when eight background events are both observed and expected, is five events. This number must be corrected by the scanning efficiency for events which have at least three tracks in the γ chambers and fit with $\chi^2\leq15$. A study of the number of type-C fits to $K_L \to \pi^0\pi^0$, found in the two independent scans, indicates an over-all efficiency of 95%. Thus the limit on the number of signal events is 5.3. A correction for the cut on m_{34} at 240 MeV, based on the shape of the distribution predicted by the Monte Carlo simulation, gives a limit of 7.5 events detected in the γ chambers. The efficiency for the detection of the 3 photons from $K_L \to \pi^0\gamma\gamma$ in the steel-plate chambers is 0.49 ± 0.05, indicating 14.5 spectrometer triggers in the kinematic region investigated. The effect of mispairing, and the misassignment of the direct photon to the spectrometer γ ray, is included in the Monte Carlo fitting efficiency since treatment of simulated events exactly paralleled that for the true data. The efficiency study of the spectrometer acceptance of $\pi^0\gamma\gamma$ decays indicates a 44% probability for the detected spectrometer γ ray to have a transverse momentum greater than 165 MeV/c. Thus the limit of 14.5 events in this region gives $N_{\pi\gamma\gamma}=33$ spectrometer events over the entire detected $P_\perp$ spectrum. Normalization is obtained from the 3π data as discussed in Sec. IV. Thus from Eq. (21), (25), and (26), we have

$$\frac{\Gamma(K_L \to \pi^0\gamma\gamma)}{\Gamma(K_L \to \pi^0\pi^0\pi^0)} < \frac{N_{\pi\gamma\gamma}}{N_{3\pi}} \frac{[\frac{1}{4}(6+2R')]}{} \frac{\epsilon_{3\pi}}{\epsilon_{\pi\gamma\gamma}} < 1.1\times10^{-3}. \quad (44)$$

The spectrometer efficiency $\epsilon_{\pi\gamma\gamma}$ for the $\pi^0\gamma\gamma$ mode is given in Table II. Using the branching ratio

$$\Gamma(K_L \to 3\pi^0)/\Gamma(K_L \to \text{all modes}) = 0.209 \pm 0.011,^{9}$$

and Eq. (44), we obtain

$$\Gamma(K_L \to \pi^0\gamma\gamma)\Gamma(K_L \to \text{all modes}) < 2.3 \times 10^{-4}, \quad (45)$$

and using $\Gamma(K_L \to \pi^0\pi^0)/\Gamma(K_L \to \pi^0\pi^0\pi^0) = (4.6 \pm 1.1) \times 10^{-3}$,

$$\Gamma(K_L \to \pi^0\gamma\gamma)/\Gamma(K_L \to \pi^0\pi^0) < 24\%, \quad (46)$$

both with 90% confidence.

VIII. CONCLUSIONS AND DISCUSSION

At the time of writing of this paper there are four other published values of $|\eta_{00}|$.[13] These are given in Table VI. Comparing our result $|\eta_{00}| = (2.2 \pm 0.3) \times 10^{-3}$ with the world average for $|\eta_{+-}| = (1.92 \pm 0.04) \times 10^{-3}$,[11] we agree with the prediction that $|\eta_{00}| \approx |\eta_{+-}|$ which would be expected if the CP violation were essentially in the mass matrix ($\epsilon' \ll \epsilon$). The superweak theory of Wolfenstein,[14] for example, predicts $\epsilon' = 0$ precisely. Our result, when combined with measurements of other CP-violation parameters of K_L decay,[15] satisfies the Wu-Yang triangle relation.[16]

Our technique in measuring the $K_L \to \pi^0\pi^0$ rate has been quite different from other measurements. Whereas the principal difficulty encountered in all other measurements has been separation of the $2\pi^0$ events from $3\pi^0$ events, with our technique the separation is simple and entirely objective. For the class of events in which all four γ rays were observed (type C), the signal is virtually free of background as can be seen in Fig. 6. Our principal difficulties have been with the normalization of the events. In particular, we have been forced to calculate efficiencies. While we have complete confidence that these calculations have been correctly done and the errors properly assigned, a calculation is always inferior to a direct measurement. Comparing the yield of $K_L \to 2\pi^0$ to $K_S \to 2\pi^0$ by means of a regenerator was impossible because of the high neutron flux in the beam. Nevertheless, the technique is powerful and we are in the process of repeating the experiment under circumstances where all efficiencies are directly measured, and where significant statistical improvement is expected.

TABLE VI. Values of $|\eta_{00}|^2$.

$10^6 \times$value	Reference
-2 ± 7	a
4.8 ± 1.9	b
13.0 ± 4.0	c
14.1 ± 3.4	d
4.9 ± 1.2	This experiment

[a] D. F. Bartlett, R. K. Carnegie, V. L. Fitch, K. Goulianos, D. P. Hutchinson, T. Kamae, R. F. Roth, J. S. Russ, and W. Vernon, Phys. Rev. Letters **21**, 558 (1968).
[b] I. A. Bugadov, D. C. Cundy, G. Myatt, F. A. Nezrick, G. H. Trilling, W. Venus, H. Yoshiki, B. Aubert, P. Heusse, I. Le Dong, J. P. Lowys, D. Morellet, E. Nagy, C. Pascaud, L. Behr, P. Beillière, G. Boutang, M. Schiff, and J. Van der Velde, Phys. Letters **28B**, 215 (1968).
[c] J. M. Gaillard, W. Galbraith, A. Hussri, M. R. Jane, N. H. Lipman, G. Manning, T. Ratcliffe, H. Faissner, and H. Reithler, Nuovo Cimento **59A**, 453 (1969).
[d] R. J. Cence, B. D. Jones, V. Z. Peterson, V. J. Stenger, J. Wilson, D. I. Cheng, R. D. Eandi, R. W. Kenny, I. Linscott, W. P. Oliver, S. Parker, and C. Rey, Phys. Rev. Letters **22**, 1210 (1969).

TABLE VII. Values of $\Gamma(K_L \to \gamma\gamma)/\Gamma(K_L \to \text{all})$.

$10^4 \times$value	Reference
6.7 ± 2.2	a
7.4 ± 1.6	b
5.3 ± 1.5	c
4.7 ± 0.6	This experiment

[a] L. Criegee, J. D. Fox, H. Frauenfelder, A. O. Hansen, G. Moscat, C. F. Perdrisat, and J. Todoroff, Phys. Rev. Letters **17**, 150 (1966); revised result given in J. A. Todoroff, thesis, University of Illinois, 1967 (unpublished).
[b] J. W. Cronin, P. F. Kunz, W. S. Risk, and P. C. Wheeler, Phys. Rev. Letters **18**, 25 (1967).
[c] R. Arnold, I. A. Budagov, D. C. Cundy, G. Myatt, F. Nezrick, G. H. Trilling, W. Venus, H. Yoshiki, B. Aubert, P. Heusse, E. Nagy, and C. Pascaud, Phys. Letters **28B**, 56 (1968).

The value for the branching ratio $\Gamma(K_L \to \gamma\gamma)/\Gamma(K_L \to \text{all}) = (4.7 \pm 0.6) \times 10^{-4}$ is in good agreement with other determinations as given in Table VII.

Finally the upper limits $\Gamma(K_L \to \pi^0\gamma\gamma)/\Gamma(K_L \to \text{all}) < 2.3 \times 10^{-4}$ and $\Gamma(K_L \to \gamma\gamma)/\Gamma(K_S \to \text{all}) < 0.02$ represent the only experimental information concerning these decay modes at the present time.

ACKNOWLEDGMENTS

We wish to thank Professor M. White, Dr. W. Wales, and the entire operations crew at the Princeton-Pennsylvania Accelerator for their cooperation and support during the experiment. The assistance of Dr. P. Wheeler, Dr. P. Kunz, Dr. W. Risk, B. Knapp, M. Shochet, and A. Nathan is also gratefully acknowledged. We are also grateful to many members of the staff at Palmer Physical Laboratory and the Elementary Particles Laboratory.

APPENDIX A

In order to provide additional confirmation that the events with $P_\perp < 165$ MeV/c arose mainly from the decays $K_L \to \pi^+\pi^-\pi^0$ and $K_L \to \pi^0\pi^0\pi^0$, an effort was made to measure the branching ratio $\Gamma(K_L \to \pi^+\pi^-\pi^0)/\Gamma(K_L \to \pi^0\pi^0\pi^0)$ from these data. The number of $\pi^+\pi^-\pi^0$ decays was found by kinematic fitting, and after the background correction described in Sec. IV, the rest of the data were assumed to arise from $K_L \to \pi^0\pi^0\pi^0$ decays.

The γ-chamber film for 6165 events with $P_\perp < 171$

[13] The result given in J. W. Cronin, P. F. Kunz, W. S. Risk, and P. C. Wheeler, Phys. Rev. Letters **18**, 25 (1967), has been shown to be incorrect (see Ref. 5).
[14] L. Wolfenstein, Phys. Rev. Letters **13**, 562 (1964).
[15] The parameters used are $|\eta_{+-}| = (1.92 \pm 0.04) \times 10^{-3}$ (Ref. 11), $\Phi_{+-} = (39.8 \pm 6)°$, and $\mathrm{Re}\epsilon = (1.42 \pm 0.17) \times 10^{-3}$ (Ref. 4).
[16] T. T. Wu and C. N. Yang, Phys. Rev. Letters **13**, 380 (1964).

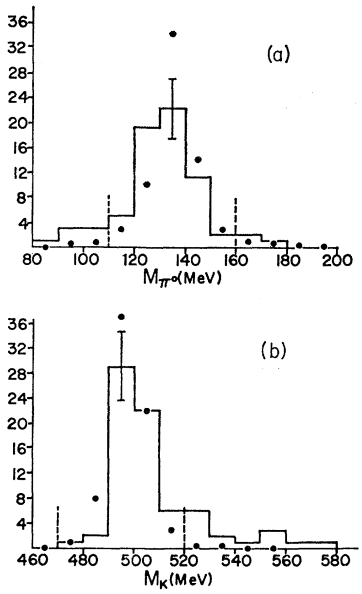

FIG. 33. (a) Distribution of fitted π^0 mass for candidates to the decay $K_L \to \pi^+\pi^-\pi^0$. (b) Distribution of fitted K mass for candidates to the decay $K_L \to \pi^+\pi^-\pi^0$. In each plot, • denotes the Monte Carlo prediction, and the region between the dashed lines is the acceptable mass region.

MeV/c[17] was searched for $\pi^+\pi^-\pi^0$ decays which appeared as two charged-particle tracks and one γ-ray track. The efficiency for complete detection of these decays was rather low because of the low Q of the reaction. In addition, the high accidental rates meant that some $\pi^+\pi^-\pi^0$ events appeared to have four tracks in the γ chambers and were lost from the scan. Also, some of the three-particle events which were retained had two particles from the decay together with an accidental track. In all, 184 events with exactly two charged tracks and one γ-ray track were found and measured. These events were subjected to a two-constant fit to the hypothesis $K_L \to \pi^+\pi^-\pi^0$. The best decay point along the trajectory of the spectrometer γ ray was found by minimizing a χ^2 statistic. The statistic was based on the mass of the decaying particle and the mass of the particle decaying to two γ rays. A requirement that all track momenta be positive and that the fitted decay point be no more than 2 in. outside the beam volume reduced the number of candidates to 79. The kinematically interesting features of the fit are shown for these 79 events in the π^0 and K_L mass plots of Fig. 33. There are 55 events in the region $110 \leq m_\pi < 160$ MeV and $470 \leq m_K < 520$ MeV.

These 55 events are used to compute the branching ratio. Corrections are necessary for the (83±8)% scanning efficiency, the (55±3)% probability of having no accidental tracks, and the 23% probability for a $\pi^+\pi^-\pi^0$ decay detected in the spectrometer to have two charged pions and the second γ ray detected, and for the event to fit in the required kinematic region. These efficiencies indicate that $N_{+-0}=531\pm90$ spectrometer triggers arose from $K_L \to \pi^+\pi^-\pi^0$. When the original 6165 events are corrected for background as described in Sec. IV, one expects $N_{3\pi}=5603$ events from 3π decay. The relative over-all spectrometer efficiencies for the two modes is $\epsilon_{+-0}/\epsilon_{000}=0.179$. This includes the fact that there are six γ rays available from $3\pi^0$ decay, and only two from $\pi^+\pi^-\pi^0$ decay. Also, the γ-ray energy spectrum for $\pi^+\pi^-\pi^0$ decay is modulated by a matrix element

$$|M|^2=1-0.48\left(\frac{m_K T_{\max}}{m_{\pi^0}{}^2}\right)\left(\frac{2T_0}{T_{\max}}-1\right),$$

where T_0 is the kinetic energy of the π^0 in the K_L c.m. system, and $T_{\max}$ is the maximum value of T_0. The $E_{\text{c.m.}}$ spectrum for $3\pi^0$ decay follows phase space (Fig. 1). Thus,

$$\frac{\Gamma(K_L \to \pi^+\pi^-\pi^0)}{\Gamma(K_L \to \pi^0\pi^0\pi^0)}=\frac{N_{+-0}}{N_{3\pi}-N_{+-0}}\frac{\epsilon_{000}}{\epsilon_{+-0}}=0.58\pm0.10.$$

This result is to be compared with the result given in Ref. 9 of 0.60±0.03.

APPENDIX B

The details of the regeneration process have been discussed at length elsewhere.[18,19] We consider here the results pertinent to the search for $K_S \to \gamma\gamma$.

An initial state $|K_L\rangle \sim (|K^0\rangle - |\bar{K}^0\rangle)/\sqrt{2}$, after traversing a medium with different absorption characteristics for the $|K^0\rangle$ and $|\bar{K}^0\rangle$ components, becomes

$$\psi(l) \sim (|K_L\rangle + \rho e^{-(\frac{1}{2}+i\delta)l}|K_S\rangle)e^{-\frac{1}{2}N\sigma_T L},$$

where l is the distance downstream from the regenerator measured in K_S decay lengths and ρ is the regenerated K_S amplitude. The other quantities are defined below.

The $|K_S\rangle$ intensity immediately after the regenerator is

$$I_{\text{coh}}=|\rho|^2 e^{-N\sigma_T L}$$
$$=(\lambda\Lambda N)^2|f_{21}(0^0)|^2\Phi e^{-N\sigma_T L},$$

with the following values:

$\rho=[i\lambda\Lambda N f_{21}(0^0)/(\frac{1}{2}+i\delta)](1-e^{-(\frac{1}{2}+i\delta)l'})$.
$\Phi=(1+e^{-l'}-2e^{-l'/2}\cos\delta l')/(\frac{1}{4}+\delta^2)$.
λ is the K wavelength $\sim$5 fm at 250 MeV/c.
Λ is the K_S decay length $\sim$1.3 cm at 250 MeV/c.

[17] This transverse momentum limit was chosen to allow a search for $K_L \to \pi^+\pi^-\gamma$. The number of events for this study is slightly lower than the raw number of events available to normalize the $K_L \to \pi^0\pi^0$ decay. This arises from the fact that the γ-chamber film had to be available for all events in this study.

[18] R. H. Good, R. P. Matsen, F. Muller, O. Piccioni, W. M. Powell, H. S. White W. B. Fowler, and R. W. Birge, Phys. Rev. **124**, 1223 (1961).

[19] J. H. Christenson, thesis, Princeton University 1964, Elementary Particles Laboratory Report No. 34 (unpublished).

N is the number density of tungsten atoms $=6.11 \times 10^{22}$ atoms/cc. This value has been compensated for the copper impurity in the Hevimet alloy.

l' is the regenerator thickness in K_S decay lengths ~ 1.1 at 250 MeV/c.

δ is the $K_S - K_L$ mass difference in units of the K_S lifetime; $\delta = -0.463$.

L is the regenerator thickness $=1.44$ cm.

σ_T is the K_L total scattering cross section.

$f_{21}(0^0) = \frac{1}{2}[f(0^0) - \bar{f}(0^0)]$, where $f(0^0)$ and $\bar{f}(0^0)$ are the forward-scattering amplitudes for K^0 and $\bar{K}^0$ in tungsten. These amplitudes are obtained from an optical-model calculation using data for K^0- and $\bar{K}^0$-nucleon scattering. Specifically, the KN data comes from the phase shift analysis by Stenger *et al.*[20] of K^+-deuterium scattering. They find an $I=0$ scattering length of $A_0 = 0.04 \pm 0.04$ fm, and an $I=1$ scattering length of $A_1 = -0.31 \pm 0.01$ fm. The $\bar{K}N$ data comes from the study by Kim[21] of K^--p scattering. He finds

$$A_0 = (-1.67 \pm 0.04) + i(0.71 \pm 0.04),$$
$$A_1 = (-0.07 \pm 0.06) + i(0.68 \pm 0.03).$$

In addition to the coherent regeneration discussed above, K_S are also produced by elastic scattering of the K^0 and $\bar{K}^0$ components, because the scattering amplitudes differ for the two states. In general, multiple nuclear scatterings are possible and the resulting angular distribution is given by[18]

$$\frac{dI}{d\Omega} = \sum_{n=1}^{\infty} B_n(P_K) G_n(P_K, \theta),$$

$$B_n = e^{-NL\sigma_T} \frac{(NL\sigma_D)^n}{n!} |f_{21}(0)|^2 \left(\frac{n(1-e^{-l'})}{l' |f_{22}(0)|^2} + (N\lambda\Lambda)^2 \Phi + \frac{n(n-1)\Phi}{l'^2 |f_{22}(0)|^2} - \frac{nN\Lambda\sigma_T\Phi}{l' |f_{22}(0)|^2} \right).$$

The coefficients B_n denote the contribution of terms associated with n nuclear scatterings, and

$$G_n = (1/2\pi n b^2) \exp(-\theta^2/2nb^2).$$

[20] N. J. Stenger, W. E. Slater, D. H. Stork, H. K. Ticho, G. Goldhaber, and S. Goldhaber, Phys. Rev. **134**, B1111 (1964).

[21] J. K. Kim, thesis, Columbia University, 1966 (unpublished).

TABLE VIII. Regeneration data.[a]

P_K (MeV/c)	$f_{21}(0^0)$ (F)	$f_{22}(0^0)$ (F)	b (mrad)	σ_T (b)	σ_{inel} (b)	$10^3 \times I_{\text{coh}}$	$I_{\text{inc}}/I_{\text{coh}}$
150	1.98	22.2	238	3.66	1.90	0.062	6.82
250	6.95	35.4	156	3.41	1.51	0.393	7.79
350	11.1	43.3	113	2.93	1.43	0.635	7.44
450	14.2	49.7	87	2.59	1.42	0.694	7.11
weighted					1.57	0.410	7.39

[a] These data are for the $\frac{1}{2}$-in. Hevimet regenerator used in the $K_S \to \gamma\gamma$ study. The parameters are defined in Appendix B.

The acceptance of the apparatus is constant over the angles involved in this problem, so that to obtain the ratio total incoherent to coherent regeneration one can integrate over solid angle and sum the above series to obtain

$$\frac{I_{\text{inc}}}{I_{\text{coh}}} = e^{NL\sigma_D} \left[1 + \frac{2\pi b^2}{\lambda^2} \left(\frac{(1-e^{-l'})}{N\Lambda\Phi} + \sigma_D - \sigma_T \right) \right] - 1,$$

where

$$\sigma_D = 2\pi b^2 |f_{22}(0^0)|^2$$

and

$$f_{22}(\theta) = \tfrac{1}{2}[f(\theta) + \bar{f}(\theta)].$$

The angular dependence of $|f_{21}(\theta)|^2$ and $|f_{22}(\theta)|^2$ is assumed to be Gaussian with the same width parameter b applying to the two distributions.

The results for several K_L momenta are given in Table VIII. The last line of the table is obtained by weighting previous entries by the K_L momentum spectrum. This spectrum has been corrected for the discrepancy between the observed and the Monte Carlo TOF spectra, as discussed in Sec. IV. It also includes a cutoff at 450 MeV/c corresponding to the 10 nsec TOF cut made on the data.

These results can be compared with those of Kamae[22] obtained for the higher-momentum range 400–1000 MeV/c. His results agree with experimental data in the region 700–1000 MeV/c. At 450 MeV/c the regeneration scattering amplitude $f_{21}(0°)$ agrees with Kamae[22] to 3%. The diffraction scattering amplitude $f_{22}(0°)$ is higher by 18%.

[22] T. Kamae, thesis, Princeton University, 1968, Elementary Particles Laboratory Report No. 45 (unpublished).